**TASK 7 REPORT**

**PASSIVE FORCE-DEFLECTION TESTS FOR 45° SKEWED ABUTMENTS – UNCONFINED**

**BACKFILL AND BACKFILL WITH MSE WINGWALLS**

*Prepared By*

Kyle M. Rollins, Professor, Civil & Env. Engrg Dept., Brigham Young Univ., 368 CB, Provo, UT 84602, (801)
422-6334, rollinsk@byu.edu

Ian Oxborrow, Research Asst., Civil & Env. Engrg Dept., Brigham Young Univ., 368 CB, Provo, UT 84602;
i.oxborrow@gmail.com

Kyle Smith, Research Asst., Civil & Env. Engrg Dept., Brigham Young Univ., 368 CB, Provo, UT 84602,
kyle.smith@byu.net

Amy Fredrickson, Research Asst., Civil & Env. Engrg Dept., Brigham Young Univ., 368 CB, Provo, UT 84602,
af711.byu@gmail.com

Arthur Guo, Research Asst., Civil & Env. Engrg Dept., Brigham Young Univ., 368 CB, Provo, UT 84602,
gzifan@gmail.com

*Prepared for*

Research Division of the Utah Department of Transportation

March 5, 2014

**EXECUTIVE SUMMARY**

Accounting for seismic forces and thermal expansion in bridge design requires an accurate passive force-deflection relationship for the abutment wall. Current design codes make no allowance for skew effects on passive force; however, quarter scale lab tests indicate that there is a significant reduction in peak passive force as skew angle increases for plane-strain cases. Similar results were obtained in field tests with unconfined backfill and mechanically stabilized earth (MSE) wingwalls with skew angles of 0°, 15°, and 30°. To further explore this issue, two additional large scale field tests were conducted each with a skew angle of 45°. One test was conducted with unconfined backfill and the other with mechanically stabilized earth (MSE) wall backfill. The abutment backwall was 11-ft (3.35-m) wide by 5.5-ft (1.68-m) high and backfill material consisted of the same dense compacted sand used in previous tests. The peak passive force for the 45° skew unconfined tests was found to be 37% of the peak passive force for the 0° skew unconfined case. The peak passive force for the 45° skew MSE wall test was 27% of the peak passive force for the 0° skew MSE wall test performed last year. These results are in good agreement with the available laboratory and numerical results; however, discrepancies suggest that backfill geometry has some effect on the reduction in peak passive force with respect to skew angle. Longitudinal displacement of the backwall at the peak passive force was found to be between 3% and 4.5% of the backwall height for both tests which is consistent with previously reported values for large-scale passive force-deflection tests. Passive pressure across the backwall was initially uniform but became non-uniform at larger displacements with the higher values at the edges of the cap. The unconfined configuration moved laterally about 0.46 in. compared to 0.27 in. of transverse movement with the MSE wall configuration. In both cases these were greater lateral movements than tests completed previously at lower skew angles. Both tests had similar pile cap rotation, with the unconfined test rotating the cap 0.03° counterclockwise and the MSE wall test rotating the cap 0.04° in the same direction. Heave geometries for the 45° skew unconfined and MSE wall tests were quite typically 3% to 4% of the fill height.

# INTRODUCTION

Numerous large-scale experiments have been conducted with the intent to determine the passive force-deflection curves that might be expected for dense compacted fill behind non-skewed bridge abutments (Mokwa and Duncan 2001; Rollins and Cole 2006; Rollins et al. 2010; Rollins and Sparks 2002). Much of this research indicates that the peak passive force can be accurately predicted using the log-spiral method and is achieved at a longitudinal deflection of 3% to 5% of the backwall height (Rollins and Cole 2006). Methods approximating the complete passive force-deflection curve with a hyperbola have been developed by Shamsabadi et al. (2007) and Duncan and Mokwa (2001). However, for simplicity in design, most specifications recommend a bilinear relationship (AASHTO 2011; Caltrans 2001).

Until recently, no large-scale experiments had been conducted to determine the passive force-deflection relationships for skewed bridge abutments. Furthermore, current bridge design practices assume the peak passive force is the same for skewed bridges as for non-skewed bridges (AASHTO 2011). However, field evidence clearly indicates poorer performance of skewed abutments during seismic events (Apirakyorapinit et al. 2012; Elnashai et al. 2010; Shamsabadi et al. 2006; Unjohn 2012) and distress to skewed abutments due to thermal expansion (Steinberg and Sargand 2010). Laboratory tests performed by Rollins and Jessee (2012) and numerical analyses performed reported by Shamsabadi et al. (2006) both found that there is a significant reduction in passive force as skew angle increases. Using data obtained from these studies, Rollins and Jessee (2012) proposed the correction factor, $R_{skew}$, given by Equation (1) which defines the ratio between the peak passive force for a skewed abutment ($P_{P\text{-}skew}$) and the peak passive force for a non-skewed abutment ($P_{P\text{-}no\ skew}$) as a function of skew angle, $\theta$.

$$R_{skew} = P_{P-\ skew}\ /P_{P-no\ skew} = 8.0 * 10^{-5}\theta^2 - 0.018\theta + 1.0 \qquad (1)$$

To more fully understand the relationship between skew angle and reduction in peak passive force, large-scale tests were previously conducted to determine the passive force-deflection curves for skew angles of 0°, 15° and 30°. These tests were conducted using an existing 11-ft (3.35-m) wide by 5.5-

ft (1.68-m) high by 15-ft (4.57-m) long pile cap which has been used for a number of previously conducted lateral load and passive force-deflection tests (Rollins et al. 2010; Rollins and Sparks 2002; Strassburg 2010). For this new study, a concrete wedge was attached to the face of the existing pile cap to simulate a 45° skewed abutment.

## BACKGROUND

As outlined by Burke Jr. (1994) and shown in Figure 1, the interaction of forces at the interface between the bridge abutment backwall and soil backfill may be expressed in terms of the total longitudinal force, $P_L$, and its components normal to and transverse to the abutment. The normal force is resisted by the passive force, $P_P$ [see Equation (2)]; and the transverse, or shear force, $P_T$ [see Equation (3)], is resisted by the shear resistance, $P_R$ [see Equation (4)]. To prevent instability of the bridge caused by sliding of the abutment against the soil backfill the inequality shown in Equation (5) must be satisfied. In addition, rotation of the entire bridge can occur if the inequality in Equation (6) is not satisfied.
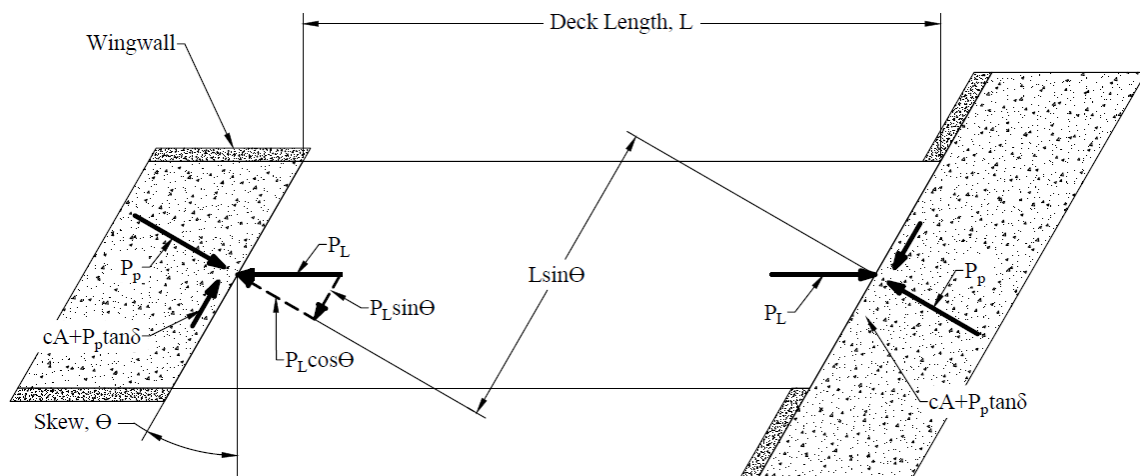


**FIGURE 1 Typical distribution of forces on a bridge with skewed abutments.**

$$P_P = P_L \cos\theta \qquad (2)$$

$$P_T = P_L \sin\theta \qquad (3)$$

$$P_R = cA + P_P \tan\delta \qquad (4)$$

$$\frac{cA + P_P \tan\delta}{F_s} \geq P_L \sin\theta \tag{5}$$

$$\frac{(cA + P_P \tan\delta)L \cos\theta}{F_s} \geq P_P L \sin\theta \tag{6}$$

where

$$\theta = \text{skew angle of backwall}$$

$$c = \text{soil cohesion}$$

$$A = \text{backwall area}$$

$$\delta = \text{angle of friction between backfill soil and abutment wall}$$

$$F_s = \text{factor of safety}$$

$$L = \text{length of bridge}$$

These equations are only strictly valid if the bridge remains stable; therefore, if the bridge rotates, the distribution of forces on the abutment backwall will likely change, rendering these equations less accurate. Based on Equation (6), Burke Jr. (1994) noted that if cohesion is ignored the potential for bridge rotation is independent of passive force and bridge length so that at a typical design interface friction angle of 22°, the factor of safety decreases to below 1.5 if bridge skew exceeds 15°.

## TEST CONFIGURATION

**Test Geometry**

The test setup for the previous lab tests is shown in Figure 2 and involved a 2 ft (0.61 m) high by 4 ft (1.22 m) wide backwall with a 2D or plane-strain backfill geometry (Rollins and Jessee 2012). In contrast, the field tests used an existing 11 ft (3.35 m) wide by 5.5 ft (1.68 m) high by 15 ft (4.57 m) long pile cap to simulate an abutment backwall as shown in Figures 3 and 4. Instead of a 2D backfill geometry, the backfill was placed in a test pit that extended a little over 5 ft (1.52 m) out from the sides of the pile cap to the edge of the test pit with transverse concrete wingwalls to allow for the development of a 3D failure geometry. The backfill extended 24 ft (7.32 m) longitudinally from the face of the pile cap and approximately 1 ft (0.30 m) below the bottom of the cap from the face to 10 ft (3.05 m) from the face to

contain the potential failure surface. Though the native soil was significantly stiffer than the backfill materials, the backfill boundaries were considered to be far enough away to not affect the development of a shear surface. Beyond 10 ft (3.05 m), the base of the backfill tapered up to be approximately even with the base of the cap to reduce the required backfill volume.

Load was applied in the longitudinal direction with two 600-kip (2,670 kN) hydraulic actuators which reacted against a sheet pile wall and two 4-ft (1.22 m) diameter drilled shafts that were coupled together by two deep beams.

A 45° wedge was attached to the front face of the pile cap for testing in the same fashion that the 15° and 30° wedges were attached the previous year as shown in Figures 3 and 4. Rollers were placed beneath the wedge to eliminate base friction resistance. The 45° skew test configuration with MSE walls is shown in Figure 4.
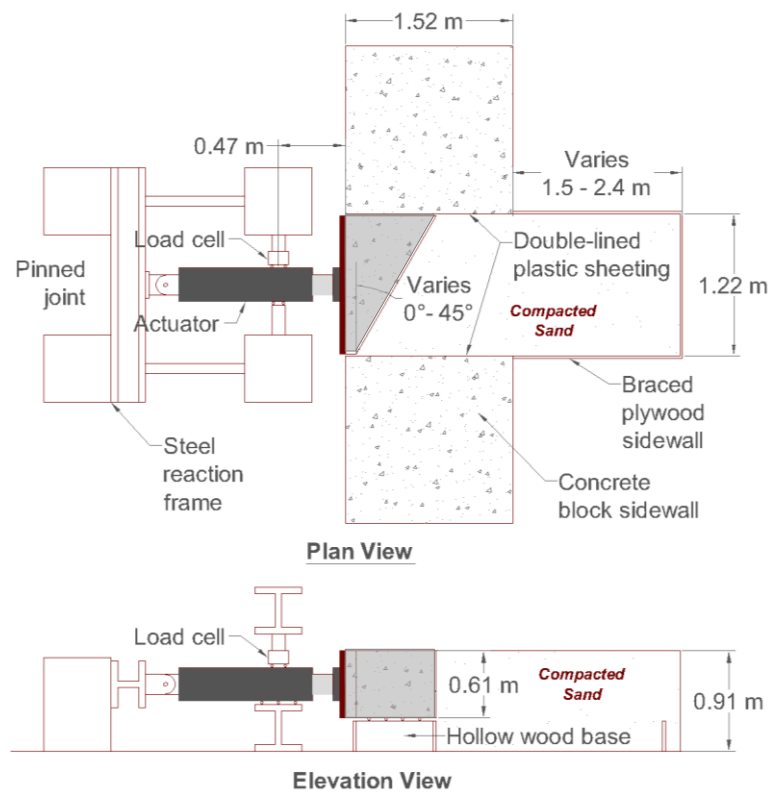


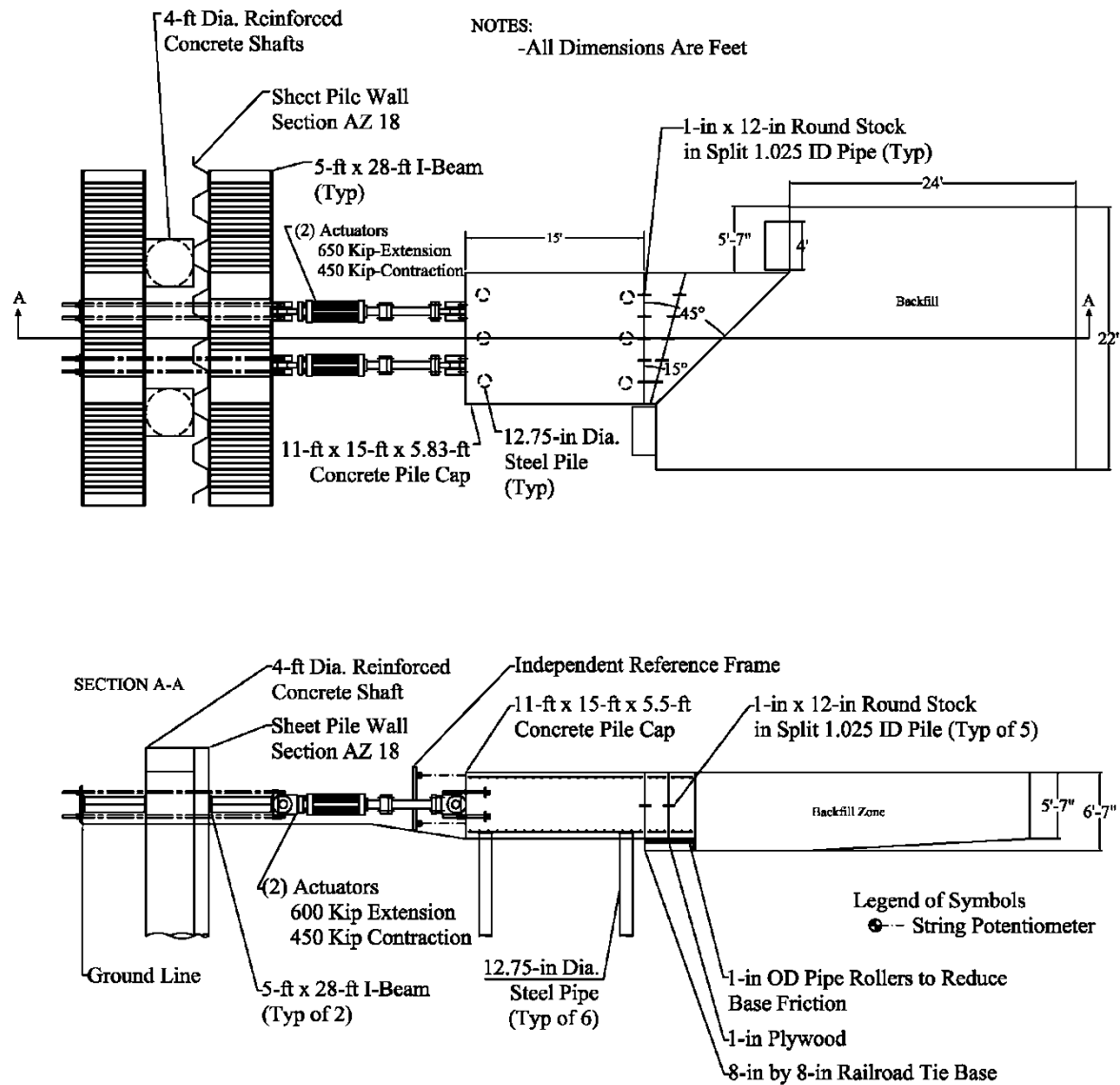**FIGURE 2 Schematic drawings of lab test layout (Rollins and Jessee 2012) (NOTE 1 m = 3.281 ft).**

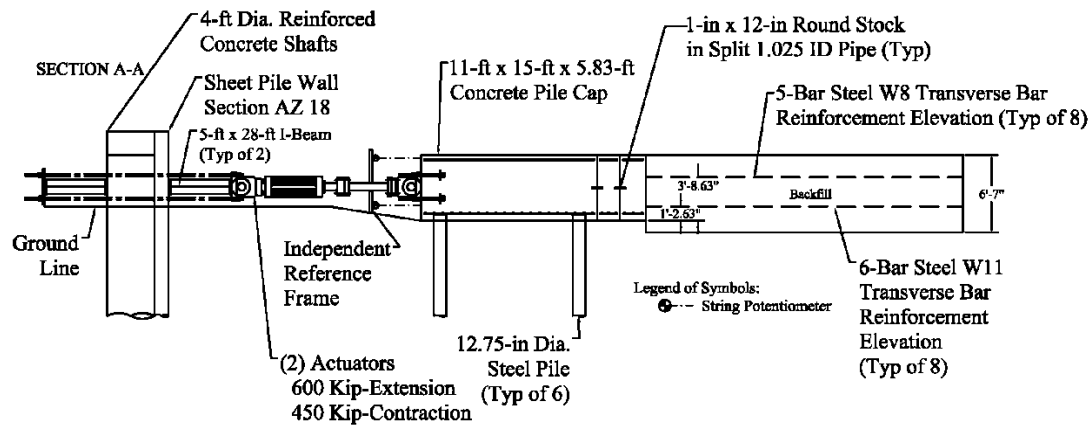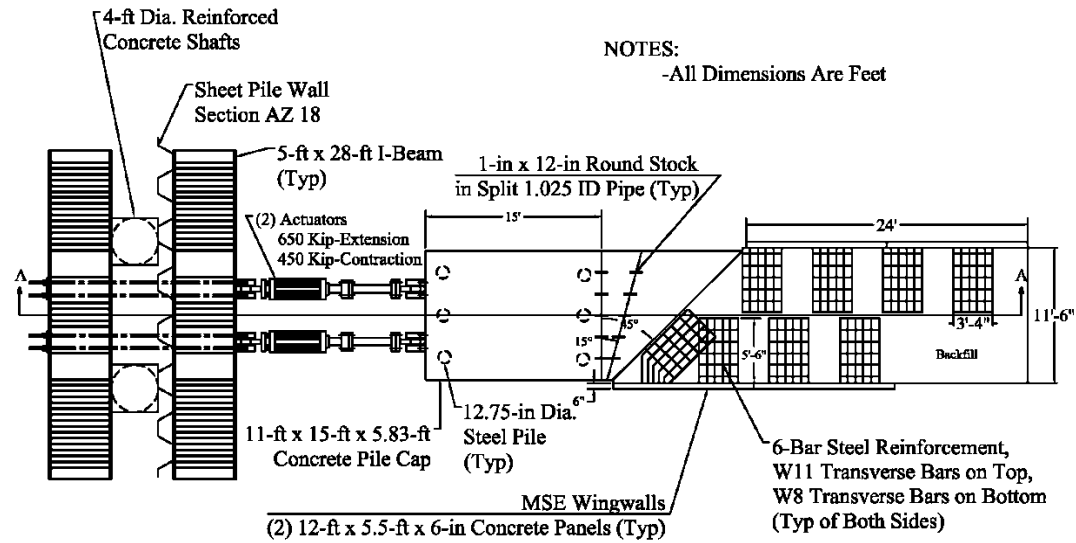**FIGURE 3 Schematic drawing of 45° skew unconfined test layout (Note: 1 ft = 0.305 m).**

4-ft Dia. Reinforced Concrete Shafts

Sheet Pile Wall Section AZ 18

5-ft x 28-ft I-Beam (Typ)

NOTES:
-All Dimensions Are Feet

1-in x 12-in Round Stock in Split 1.025 ID Pipe (Typ)

(2) Actuators
650 Kip-Extension
450 Kip-Contraction

15'

24'

A

A

45°

15°

3'-4"

11'-6"

5'-6"

6"

Backfill

12.75-in Dia. Steel Pile (Typ)

11-ft x 15-ft x 5.83-ft Concrete Pile Cap

6-Bar Steel Reinforcement, W11 Transverse Bars on Top, W8 Transverse Bars on Bottom (Typ of Both Sides)

MSE Wingwalls
(2) 12-ft x 5.5-ft x 6-in Concrete Panels (Typ)

SECTION A-A

4-ft Dia. Reinforced Concrete Shafts

Sheet Pile Wall Section AZ 18

5-ft x 28-ft I-Beam (Typ of 2)

11-ft x 15-ft x 5.83-ft Concrete Pile Cap

1-in x 12-in Round Stock in Split 1.025 ID Pipe (Typ)

5-Bar Steel W8 Transverse Bar Reinforcement Elevation (Typ of 8)

3'-8.63"

Backfill

6'-7"

1'-2.63"

Ground Line

Independent Reference Frame

Legend of Symbols:
⊕- - String Potentiometer

6-Bar Steel W11 Transverse Bar Reinforcement Elevation (Typ of 8)

(2) Actuators
600 Kip-Extension
450 Kip-Contraction

12.75-in Dia. Steel Pile (Typ of 6)

**FIGURE 4 Schematic drawing of 45° skew with MSE walls test layout (Note: 1 ft = 0.305 m).**

**Instrumentation**

Longitudinal load was measured using pressure transducers in the actuators. Longitudinal displacement of the pile cap was measured using four string potentiometers (string pots) located at each corner of the back of the pile cap and were tied to an independent reference frame. Longitudinal and transverse deflection versus depth profiles were measured using inclinometers and shape accelerometer arrays which extended approximately 40 ft (14 m) into the center pile in the North and South sides of the pile cap. The shape arrays provided data at 1 ft (0.30 m) intervals while the inclinometers provided data at 2 ft (0.6 m) intervals. Because of the time required to obtain inclinometer readings, the inclinometer measurements were only taken immediately before the start of a test and after the last deflection increment. In contrast, the shape arrays provided profiles at each deflection increment because their collection was essentially instantaneous.

A total of six "Fat Back" pressure cells manufactured by Geokon® were installed horizontally across the face of the skew wedge as shown in Figure 5. These pressure cells, also referred to as pressure plates, defined the horizontal pressure distribution at the interface with the soil as the pile cap was pushed into the backfill soil.  Five additional pressure cells were installed between the six Geokon® pressure cells to provide additional pressure measurements by Prof. Mark Talesnick of the Technion University in Israel. Data from these five pressure cells will be presented in the final report.

To measure backfill displacement a 2 ft (0.61 m) grid was painted on the backfill surface. The relative elevation of each grid intersection was measured with a survey level prior to, and after conducting each test. Northings and Eastings of each grid intersection were also measured with a total station before and after each test. Surface cracks in the backfill were also marked following the completion of each test. Where possible, a hand auger was used to drill 2-in (51-mm) diameter, vertical holes along 3 lines perpendicular to the face of the cap. These holes were then refilled and compacted with red-dyed sand. At the completion of the test a trench was excavated adjacent to each column to determine the offset in the column produced by the shear surface and the depth where this shear surface was located. Lines were

placed at the center point and at quarter points of the cap length. The center and west lines had holes dug at 2, 4, 7, and 10 ft. The east line had holes dug at 2, 4, 6, and 8 ft.



**FIGURE 5 Pile cap wedge interface.**

Following final pile cap displacement, a trench was excavated adjacent to these holes and the offset in the sand columns identified the locations of the failure surfaces. Sand columns were used for the unconfined test but not the MSE wall test.

**Geotechnical Backfill Properties**

Backfill materials consisted of a poorly-graded sand (SP or A-1-b as classified by the Unified Soil Classification System or AASHTO classification system, respectively). The particle-size distribution generally falls within the gradation limits for washed concrete sand (ASTM C33) as shown in Figure 6. Gradations before and after the test series found that the coefficient of uniformity ($C_u$) and coefficient of curvature ($C_c$) were 7.6 and 0.8 pre-test, and 9.7 and 0.7 post-test, respectively. This variability is likely

due to small differences in soil samples. For comparison, the $C_u$ and $C_c$ values from the lab tests were 3.7 and 0.7, respectively. Figure 6 also shows the soil gradation for the lab tests.
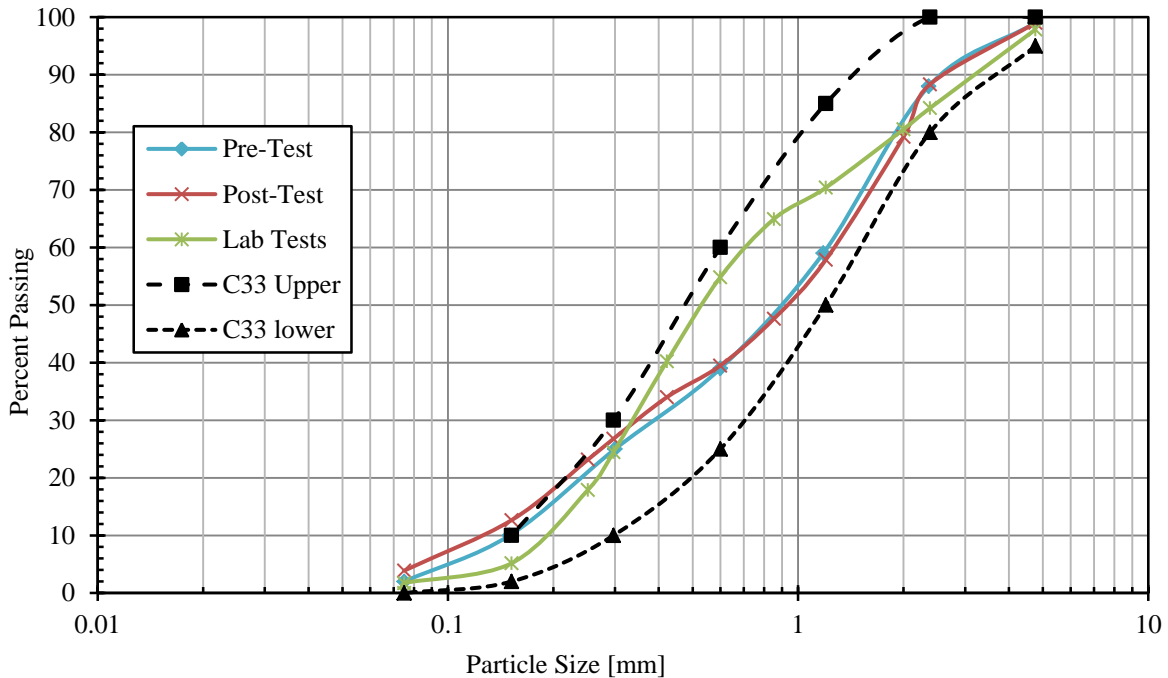


**FIGURE 6 Gradation for backfill sand relative to concrete sand gradation.**

*Unit Weight and Moisture Content*

Maximum dry unit weight according to the modified Proctor compaction test (ASTM D1557) performed prior to testing was 111.5 lbf/ft$^3$ (17.52 kN/m$^3$) and the optimum moisture content was 7.1%. The target on-site compaction level was 95% of the modified Proctor maximum. Backfill sand was placed in lifts approximately 6-in (15.24-cm) thick and compacted with a smooth-drum vibratory roller and a walk-behind vibratory plate compactor to an average density greater than approximately 95% of the modified Proctor maximum. A nuclear density gauge was used to obtain relative compaction and water content data during compaction. Relative density was estimated using the empirical relationship between relative density ($D_r$) and relative compaction (R) for granular materials developed by Lee and Singh (1971) as shown in Equation (7) where $D_r$ and R are measured in percent.

$$R = 80 + 0.2D_r \hspace{3cm} (7)$$

A summary of the soil density and water content measurements for the three tests is shown in Table 1.

The properties of the two backfills were generally very consistent. Average relative compaction, relative

density, and water content for the tests were 98.4%, 91.8%, 9.1%, respectively. For comparison purposes

the average relative compaction, relative density, and water content for the laboratory tests were 97.9%,

90%, and 8.0%, respectively (Rollins and Jessee 2012). Measured dry unit weights and water contents for

both tests at 6 in. increments throughout the backfill are displayed in Figures 7 through 10.

**TABLE 1 Summary of Compaction and Water Content Data for Both Tests**

| Backfill Soil Properties | 45⁰ Skew Uncon. Test | 45⁰ Skew MSE Test |
|---|---|---|
| **Minimum Dry Unit Weight [pcf]** | 106.5 | 107.0 |
| **Maximum Dry Unit Weight [pcf]** | 111.6 | 114.1 |
| **Average Dry Unit Weight [pcf]** | 109.1 | 109.7 |
| **Relative Compaction** | 98.3% | 98.4% |
| **Relative Density** | 91.5% | 92% |
| **Moisture Content** | 9.0% | 9.2% |
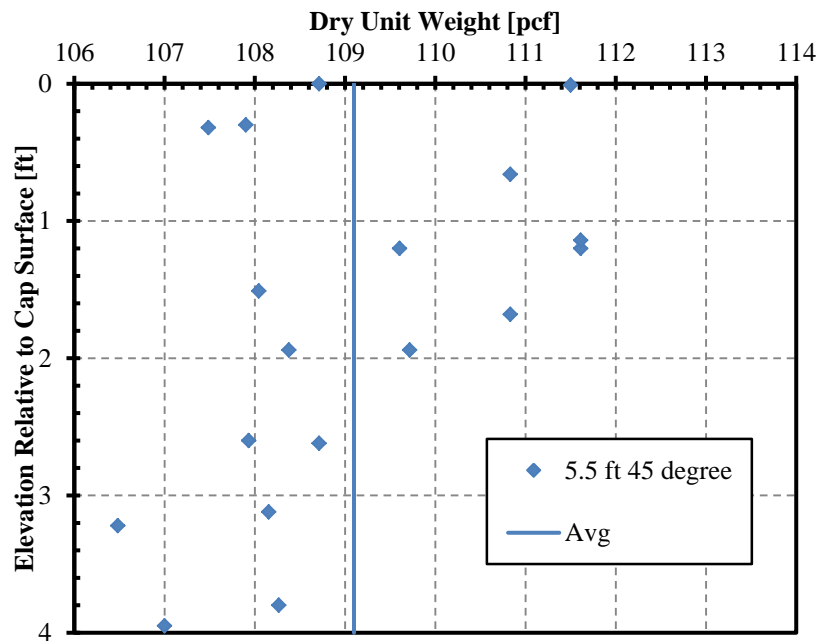


**FIGURE 7 Dry unit weight spread for unconfined test.**
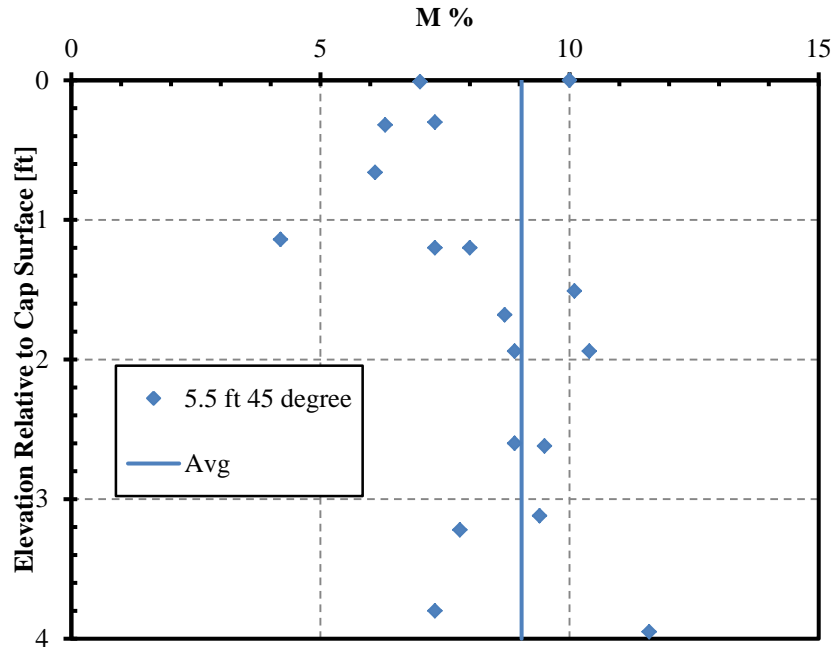
**FIGURE 8 Moisture content spread for unconfined test.**
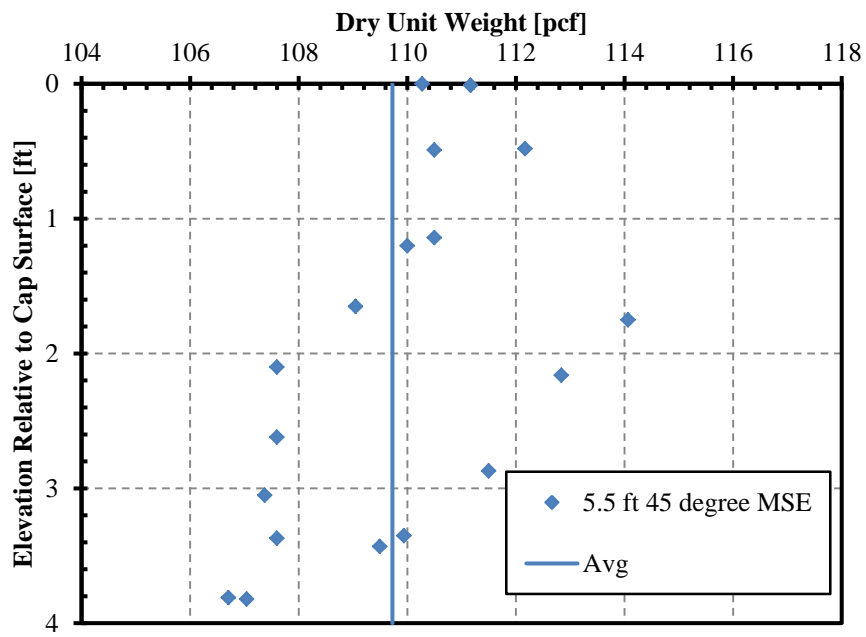


**FIGURE 9 Dry unit weight spread for MSE test.**
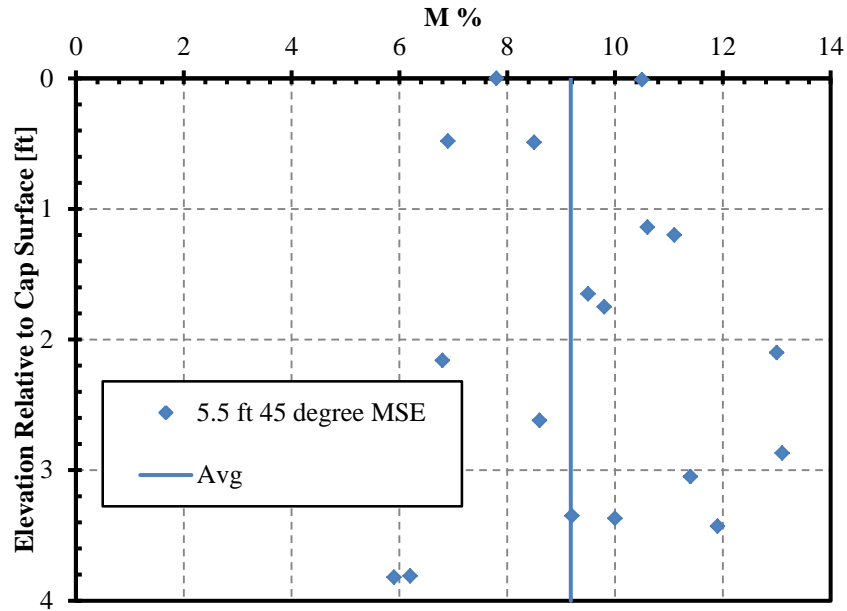
**FIGURE 10 Moisture content spread for MSE test.**

*Shear Strength*

Direct shear tests were conducted previously at the field density and moisture content values, and the drained friction angle ($\phi'$) was found to be 41° with a cohesion of 96 lbs/ft$^2$ (4.61 kN/m$^2$). Previous researchers (Rollins and Cole 2006; Rollins and Jessee 2012) conducted direct shear tests and determined that the interface friction angle ($\delta$) between similar sand and concrete was about 75% of the soil friction angle. For comparison purposes, the drained friction angle of the sand for the laboratory skew tests was 46° with a cohesion of 70 lbs/ft$^2$ (3.35 kPa) (Rollins and Jessee 2012).

**General Test Procedures**

Prior to testing with the backfill in place, a lateral load test was performed to determine the "baseline" resistance of the pile cap alone, and the pile cap with attached wedge. Because the pile cap had been previously employed for a number of tests, the baseline resistance has become relatively linear. Following the baseline test, backfill was compacted adjacent to the cap and a lateral load test was performed to obtain the total resistance. Following backfill compaction, the grid and soil columns were installed and appropriate initial measurements, including relative elevations and locations of the grid

points, were recorded. The backfill material was completely excavated and re-compacted for each individual test.

The pile cap and attached wedge was then pushed longitudinally into the backfill zone in 0.25-in (6.35-mm) increments at a velocity of 0.25 in/min (6.35 mm/min) to a final displacement of 3.25 in to 3.75 in (8.30 cm to 9.53 cm) using the two hydraulic actuators. At each 0.25-in (6.35-mm) displacement increment the load was held for approximately 2 minutes to observe the reduction in longitudinal force against the backwall as a function of time. On average, the reduction in force after 2 minutes was 7.6%.

## TEST RESULTS

### Failure Surface Geometry

Plots of the heave contours and surface cracks at the completion of the 45° skew unconfined and MSE wall tests are shown in Figures 11 and 12, respectively. Heave measurements were taken using a total station. Maximum heaves of 1.7 in (43 mm) and 1.8 in (46 mm) were measured for the unconfined and MSE tests, respectively. The location of maximum heave for both tests was observed to be near the acute corner of the pile cap (west side). In both cases maximum heave was nearly 3% of the maximum height of the backfill [5.5 ft (1.68 m)]. In contrast, for the zero skew tests the heave pattern was essentially symmetric about the centerline.

Surface cracks were minimal and spread outward from the corners of the pile cap on the unconfined backfill after 2.96 in of longitudinal displacement. For the unconfined backfill test the surface cracking was normal to the wall face on the obtuse corner but parallel to the wall face on the acute corner. For the MSE wall backfill test, the majority of cracks were observed to be longitudinal in direction after 3.5 in of pile cap longitudinal displacement. This crack pattern suggests that the MSE walls are moving outward transverse to the direction of loading and the backfill is splitting apart. Surface cracks formed as far as 22 ft from the pile cap on the MSE wall backfill while cracks were observed only as far as 4 ft from the pile cap on the unconfined backfill.
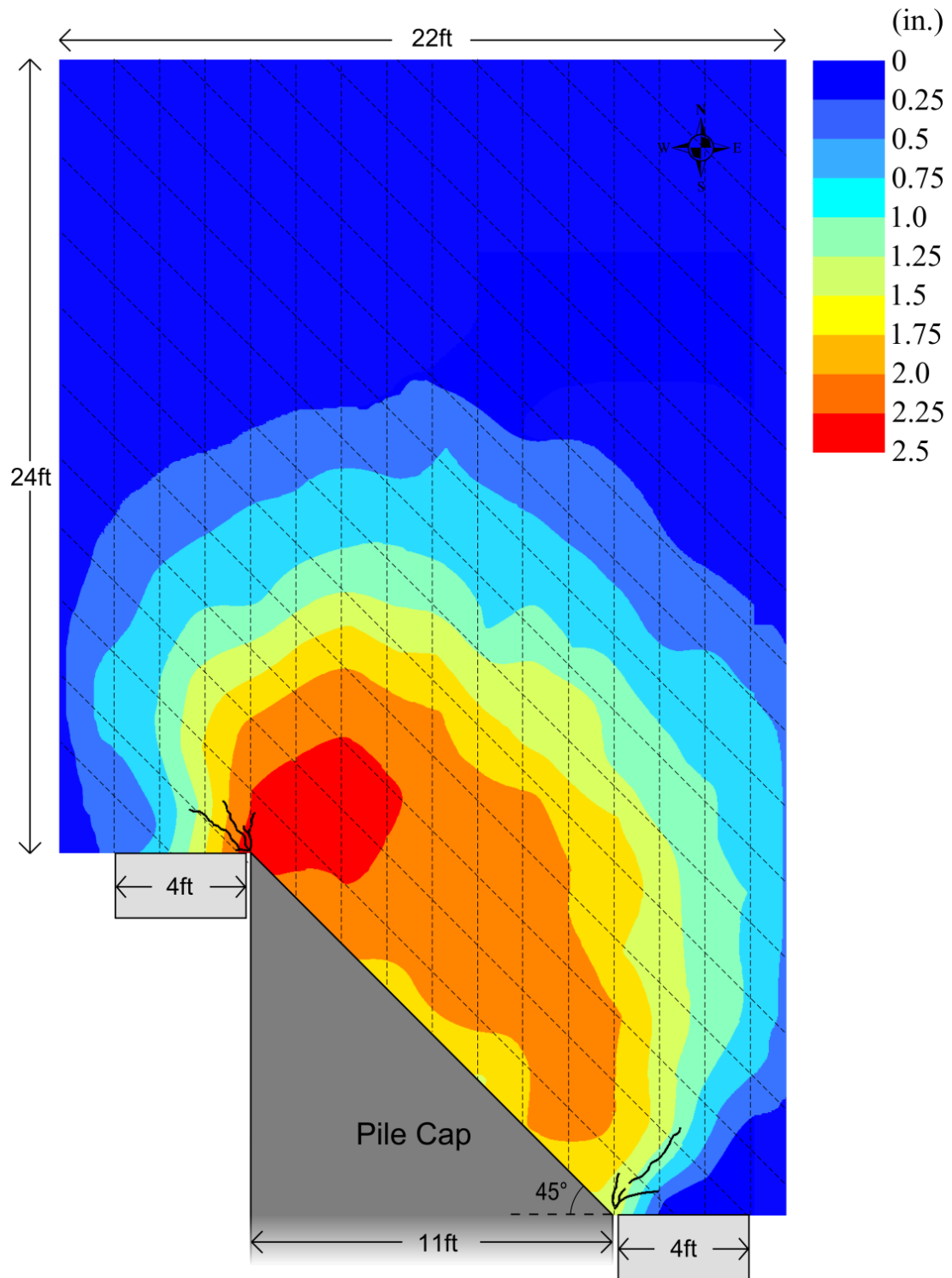
**FIGURE 11 Heave contours (units in inches) and surface cracks at 2.96 in (7.51 cm) of longitudinal displacement (test completion) for 45° skew unconfined test. Vertical and horizontal grid spacing of 2 ft. (NOTE: 1 inch = 2.54 centimeters).**
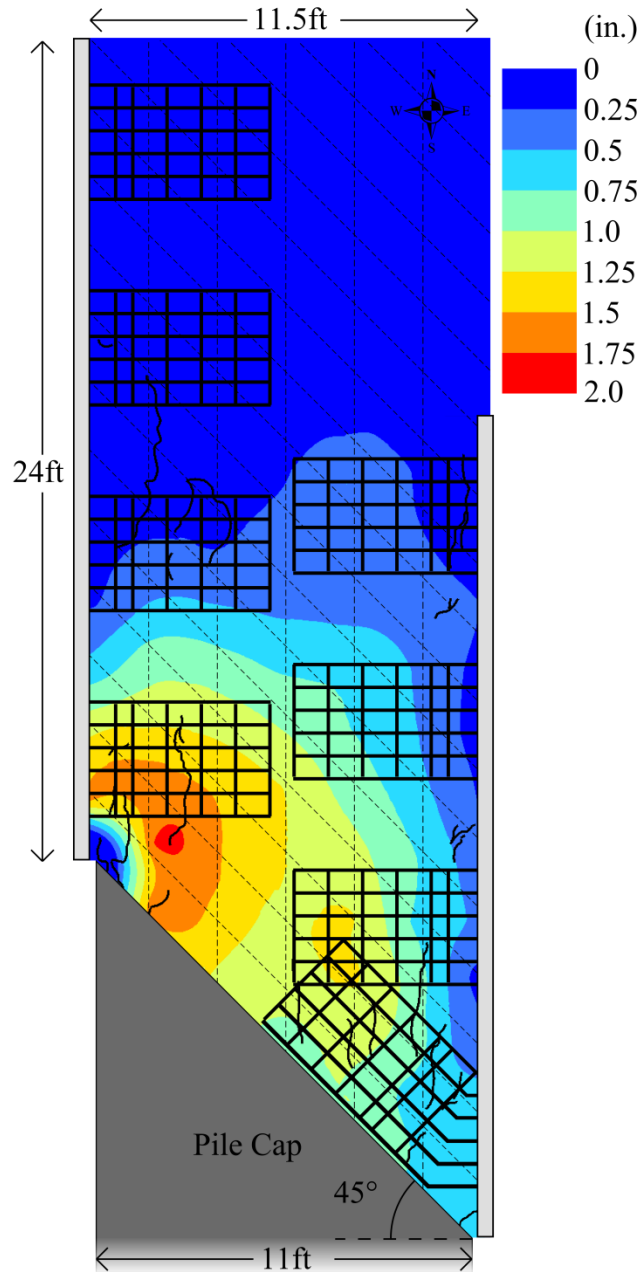
**FIGURE 12 Heave contours (units in inches) and surface cracks at 3.5 in (8.89 cm) of longitudinal displacement (test completion) for 45° skew test with MSE walls. Vertical and horizontal grid spacing of 2ft. (NOTE 1 inch = 2.54 centimeters).**

Figures 13 and 14 illustrate the horizontal (x-y) displacement of the soil based on the total station measurements at test completion. The unconfined backfill appeared to displace nearly longitudinally along with the pile cap, however, the outside edges of the backfill displaced outward or away from the

center of the backfill. The backfill confined by the MSE walls appears to have experienced more transverse displacement than the unconfined backfill. While the unconfined backfill was largely displaced parallel with the pile cap displacement, the majority of the MSE wall backfill appeared to displace perpendicular to the 45° pile cap face. As a whole, soil along the east MSE wall experienced more displacement than along the west wall.
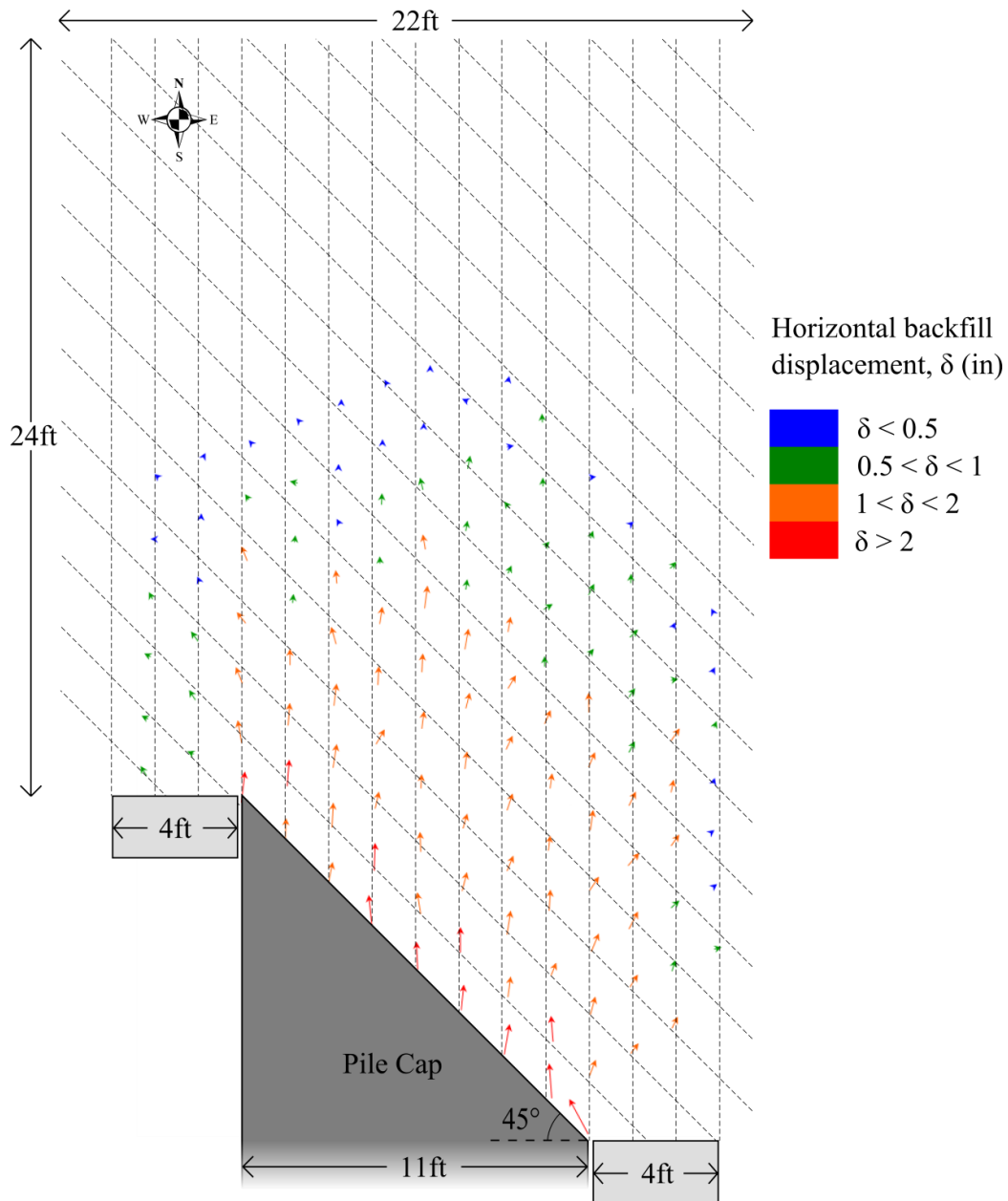


**FIGURE 13 Soil displacement for 45° skew 5.5 ft. unconfined sand backfill (Vector Scale 5:1).**
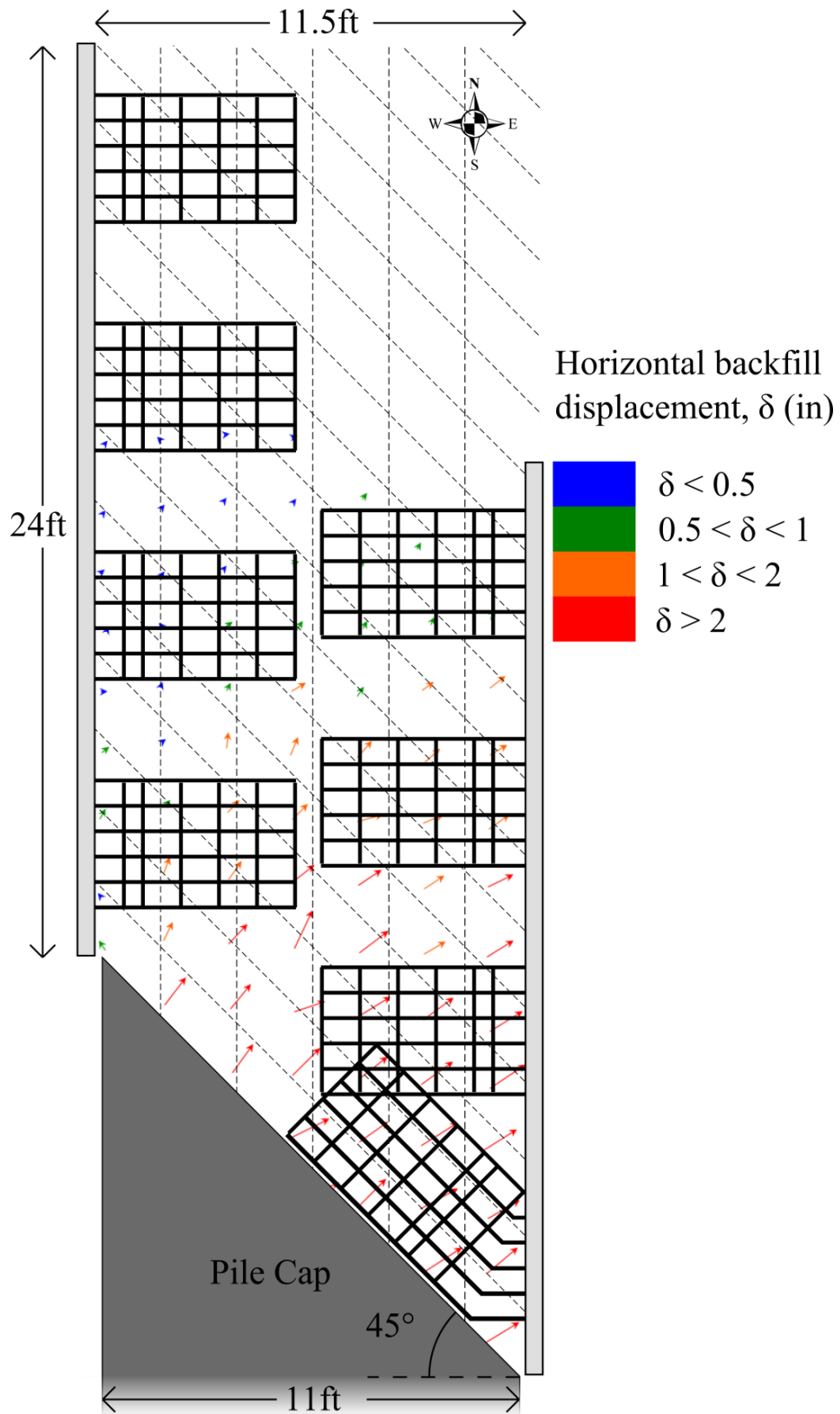
**FIGURE 14 Soil displacement for 45° skew 5.5 ft. sand backfill with MSE walls (Vector Scale 5:1).**

**Passive Force-Deflection Curves**

      Figures 15 and 16 show the passive force versus longitudinal deflection curves for the 45°

unconfined test and 45° MSE wall test, respectively along with the curves for 0°, 15°, and 30° skews

tested in 2012. The peak passive force for the unconfined test (≈170 kips) is about 35% greater than that

for the MSE wall test (≈125 kips). This appears to result from that fact that the shear planes in the

unconfined test can extend beyond the edges of the cap which increases the effective cap width as shown

subsequently. In terms of passive force per "effective" cap width the values are nearly identical (≈11.3

kips/ft of width),
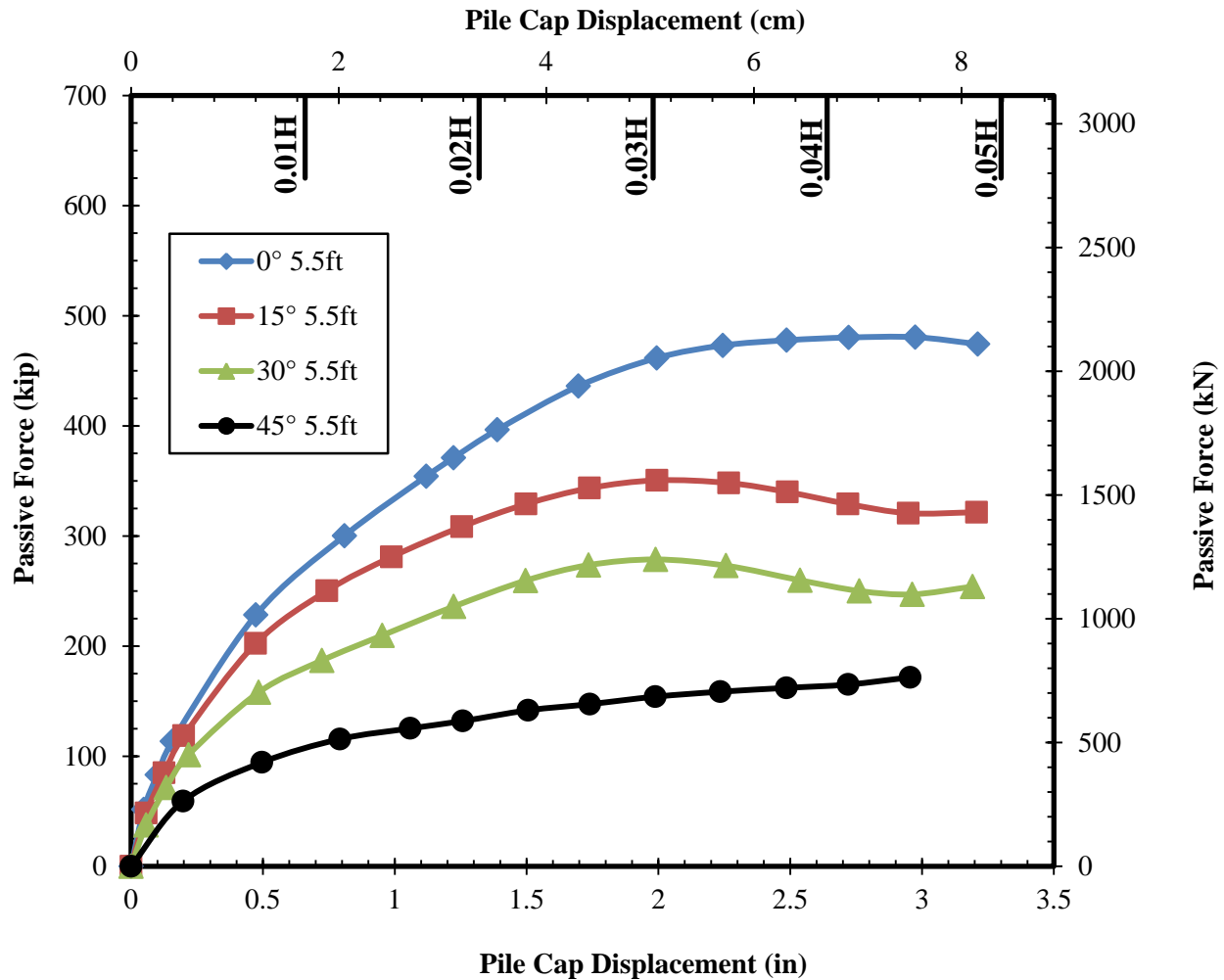


**FIGURE 15 Passive force versus longitudinal deflection for unconfined tests.**
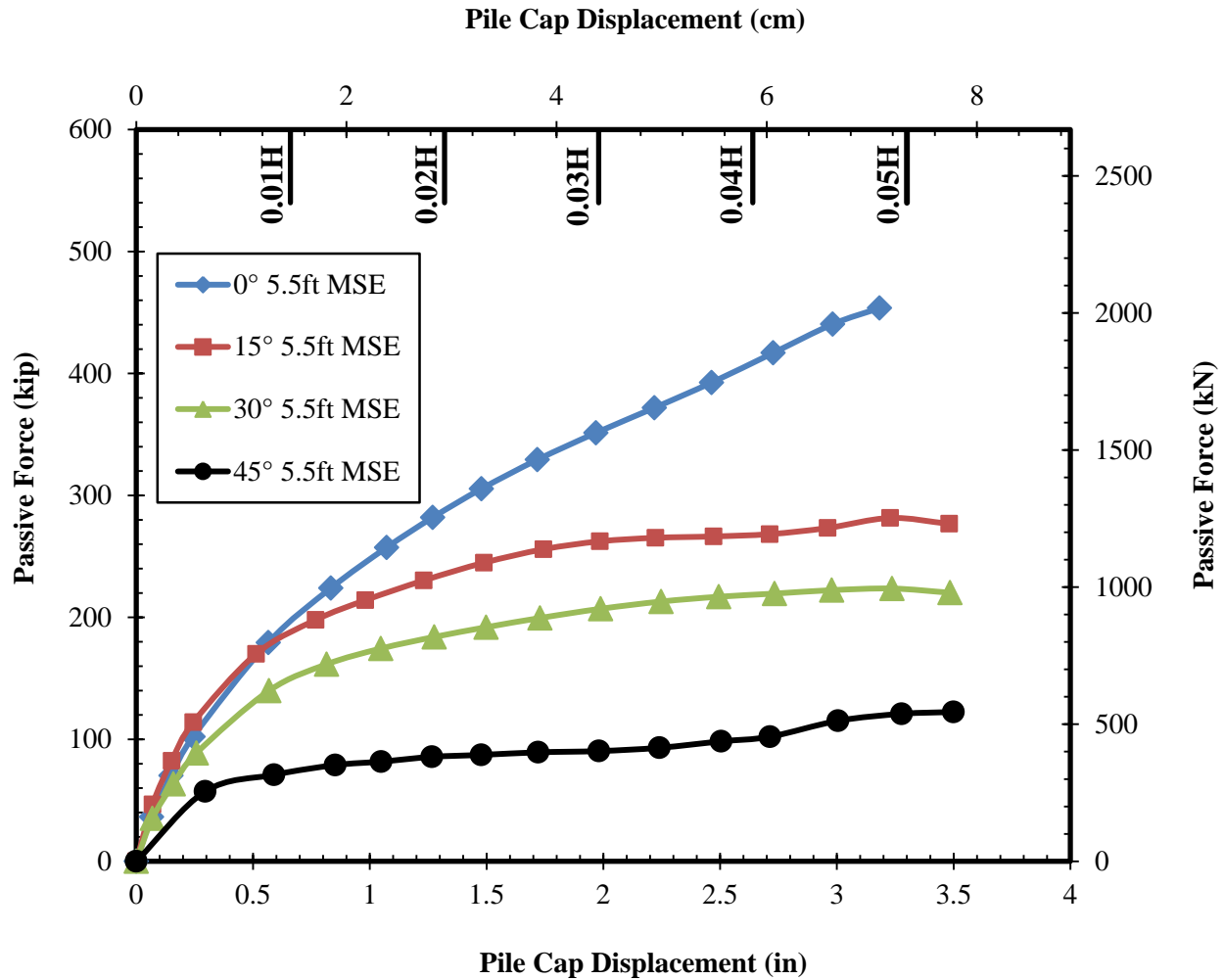
**FIGURE 16 Passive force versus longitudinal deflection for MSE wall tests.**

The total load and corresponding baseline curves for the 45° skew tests are illustrated in Figures 17 and 18. The resistance of the pile cap in the longitudinal direction is a combination of both the passive and shear resistance of the pile cap. This resistance is represented by the difference between the total and baseline curves. Normal passive force was obtained by multiplying the longitudinal resistance of the pile cap by the cosine of the skew as given by Equation (2), $P_P = P_L \cos\theta$.
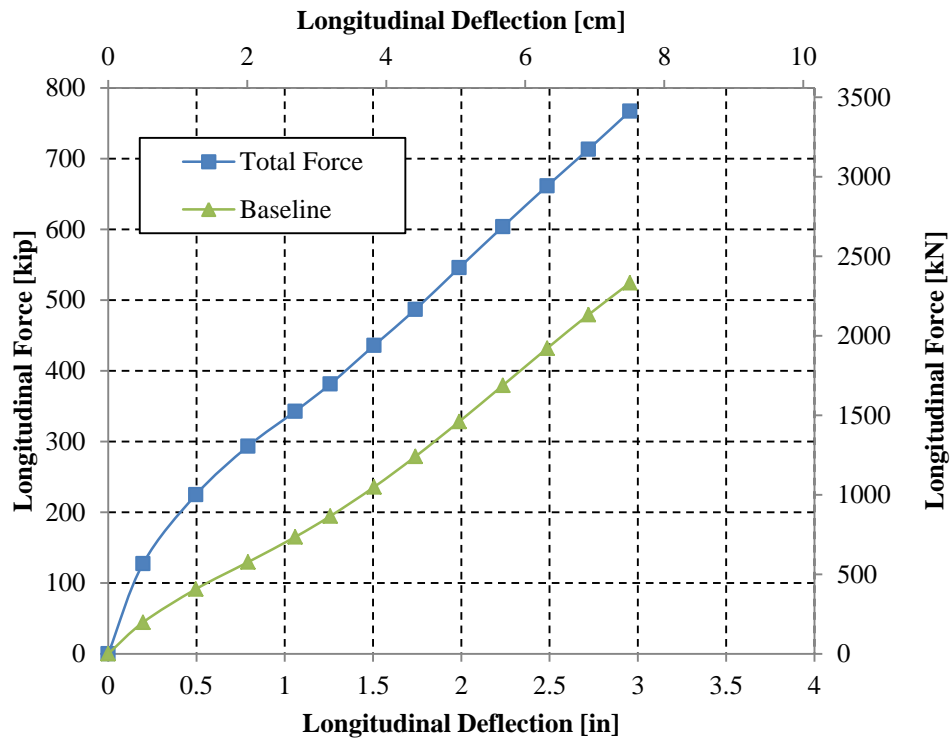
**FIGURE 17 Total load and baseline resistance for 45° skew unconfined.**
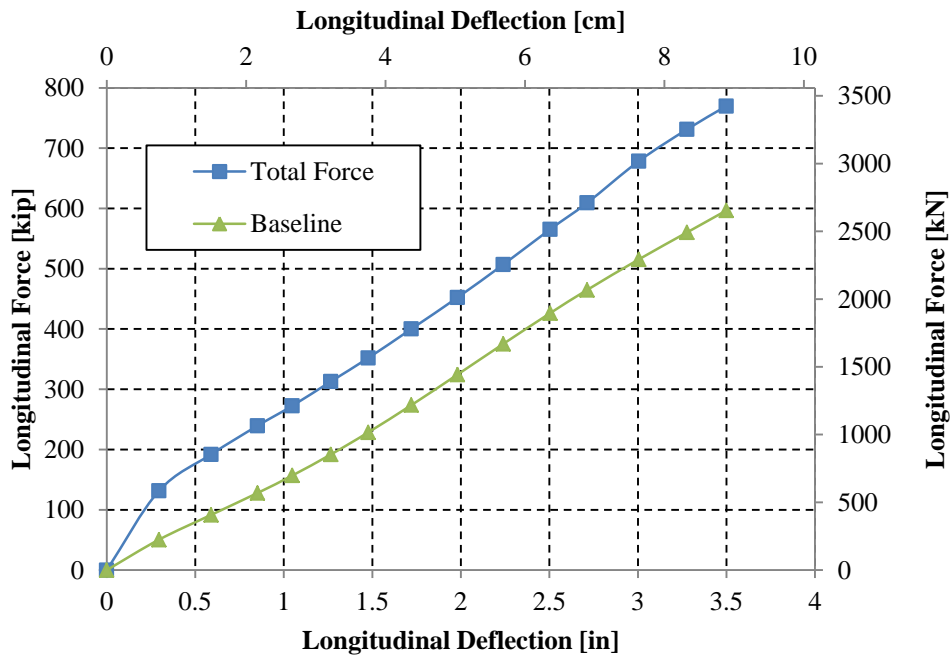


**Figure 18 Total load and baseline resistance for 45° skew with MSE walls.**

Figure 19 plots the passive force reduction factor versus skew angle for the lab tests conducted by Rollins and Jessee (2012), for the numerical models reported by by Shamsabadi et al. (2006), and for the results of this study. As can be seen from the Figure 19, Equation (1) predicts that at a skew angle of 45° the passive force reduction factor should be approximately 35% when compared to the 0° skew case. The measured reduction factors from the field tests were 37% and 27% for the 45° unconfined and MSE wall tests, respectively. The general agreement between the field test results and the numerical and lab test results suggests that 3D effects and geometry considerations may have only a small effect on the reduction in passive force with respect to skew angle as predicted by Equation (1). Although the reduction factors for the MSE tests tend to be somewhat lower, these results generally support the notion that the equation for a reduction factor with respect to skew angle is generally applicable.
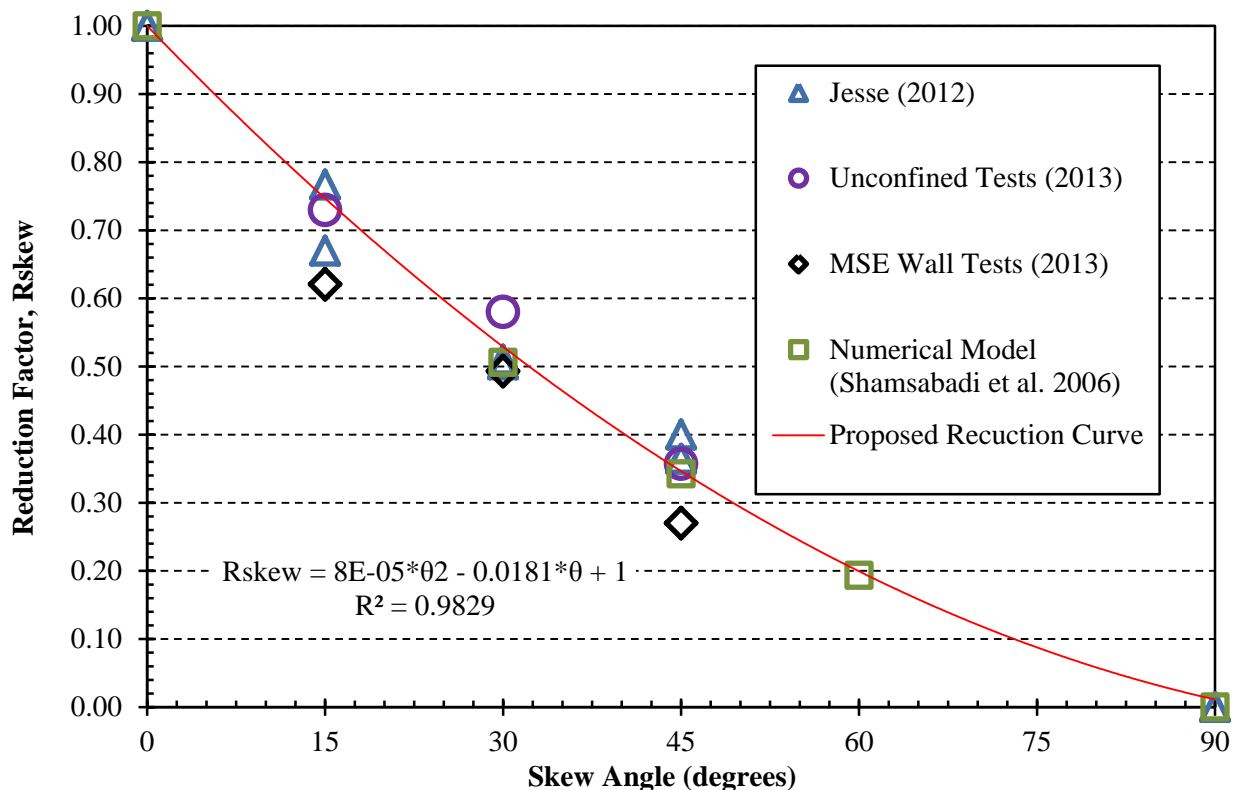


**FIGURE 19 Reduction factor, $R_{skew}$ (passive force for a given skew angle normalized by passive force with no skew) plotted versus skew angle based on lab tests (Rollins and Jessee 2012), numerical analyses (Shamsabadi et al. 2006) and results from field tests in this study.**

## Pile Cap Displacement vs. Depth

Figure 20 provides longitudinal deflection versus depth profiles obtained from both an inclinometer and a shape accelerometer array (SAA) for the 45º skew test with unconfined backfill. Both profiles represent pile cap behavior for the final longitudinal displacement of the test. Figure 21 shows the same plots for the 45º skew test with MSE walls. The depths are referenced to the top of the cap. The average deflection measured by the string pots at two elevations on the pile cap are also shown in Figure 21 for comparison purposes. The graphs demonstrate that the measurements for the three systems were reasonably accurate and aligned with each other. The percent difference between the inclinometer and shape array profiles from the top of the cap to a depth of 15 ft (4.6 m) ranges between 0.1 and 3.2% for the 45° skew unconfined test with an average of about 0.5%. The corresponding percent difference was between 0.07 and 12.8% for the 45° skew MSE wall test with an average of about 4.7%. The displacements below a depth of 15 ft (4.6 m) are very small and because of greater error in the shape arrays for displacements less than 0.25 inch (Rollins et al. 2009), error percent values in this zone are not particularly meaningful. Similar good agreement was obtained between the shape array and string potentiometers for the other displacement levels.
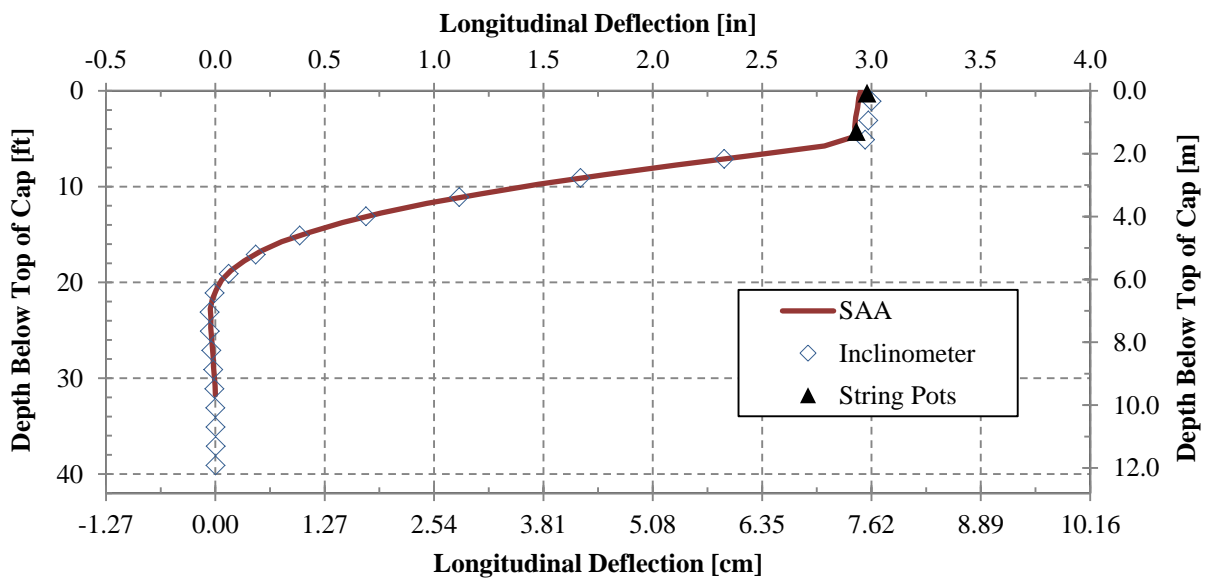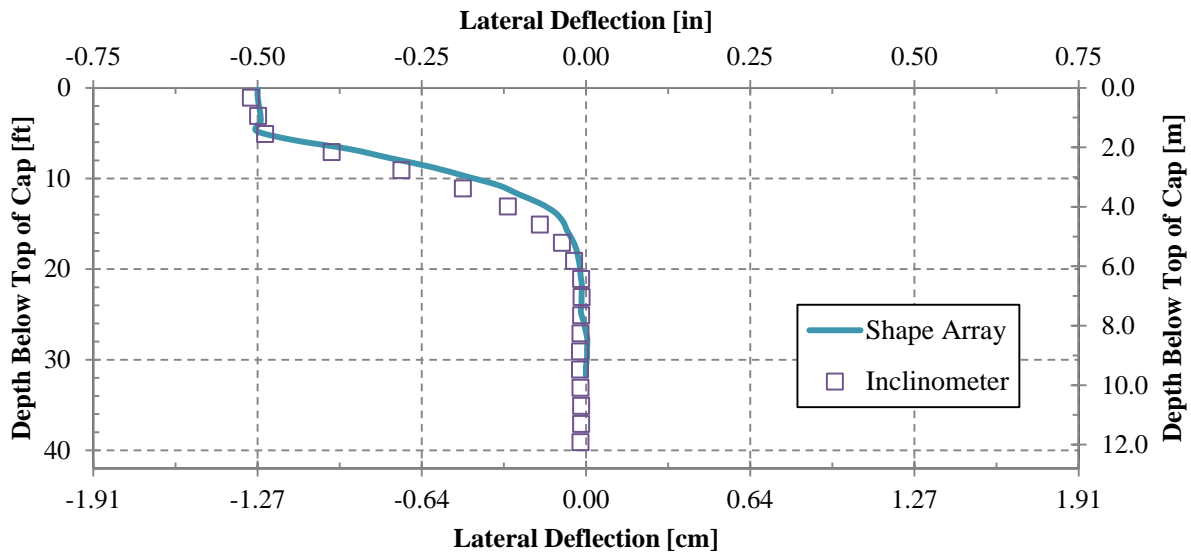


**FIGURE 20 North 5.5-ft backfill 45° skew final deflection; comparing inclinometer, shape array, and string potentiometers.**
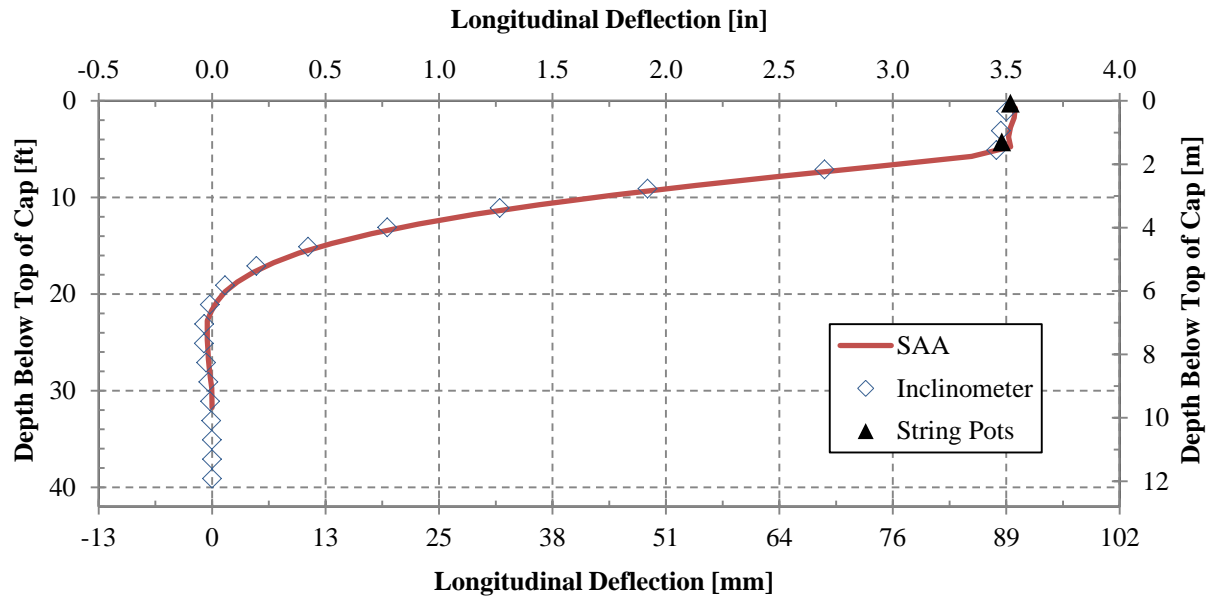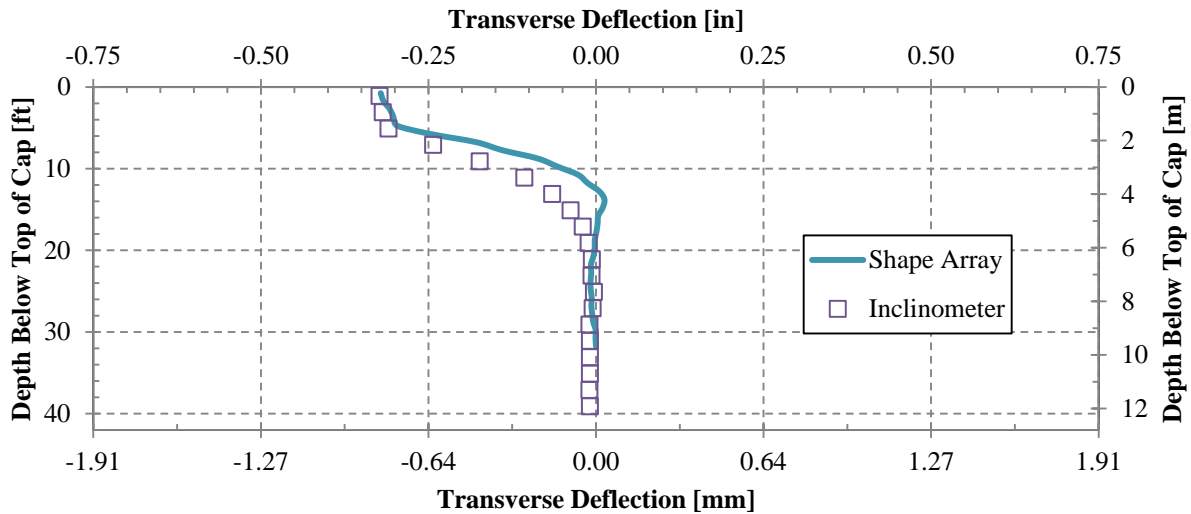
**FIGURE 21 North 5.5-ft backfill 45° skew MSE wall final deflection; comparing inclinometer, shape array, and string potentiometers.**

The measurements indicate a relatively linear deflection profile within the pile cap and small cap rotations. Below the base of the cap, the piles deflect in a non-linear fashion with the deflections reaching a point of counterflexture at depth of approximately 21 ft (6.3 m) and a point of fixity at about 31 ft (9.45 m). Agreement between the north and south inclinometers was generally very good.

Transverse deflection versus depth profiles for the pile cap, recorded by the shape array and inclinometer, are plotted below in Figures 22 and 23. Plotted on a smaller scale, the percent error seems larger than the longitudinal error although the magnitude difference is small. However, as observed for the deflections below 15 ft (4.6 m) in the longitudinal test, the percent difference is exaggerated due to the smaller scale. The percent difference is within the error thresholds of each instrument ($\pm$1.5 mm/30 m for shape array, and $\pm$1.24 mm/30m for inclinometer (Rollins et al. 2009). Results were similar for the tests at other skew angles. Once again, the shape of the deflection profile indicates essentially linear deflection in the pile cap and very small rotations. The deflection in the piles is non-linear and decreases to zero at a deflection of about 20 ft (6 m).

**FIGURE** 22 **North 5.5-ft unconfined backfill 45° skew unconfined final deflections; comparing inclinometer and shape array.**



**FIGURE 23 North 5.5-ft unconfined backfill 45° skew MSE wall final deflections; comparing inclinometer and shape array.**

Although the inclinometer readings were only taken at the maximum deflection for each load test, shape array profiles in the longitudinal and transverse directions were obtained at each deflection increment for each test. For example, Figure 24 shows profiles of longitudinal deflection vs. depth for

each deflection increment for the 45° unconfined test. As the deflection level increases the deflection of

the pile cap remains linear but the rotation progressively increases while the depth to the point of fixity

increases. Similar curves were obtained in the transverse direction. At smaller deflection levels there are

some variations associated with the small measurement errors; however at larger deflections, the data was

accurate and useful in visualizing the pile movement.
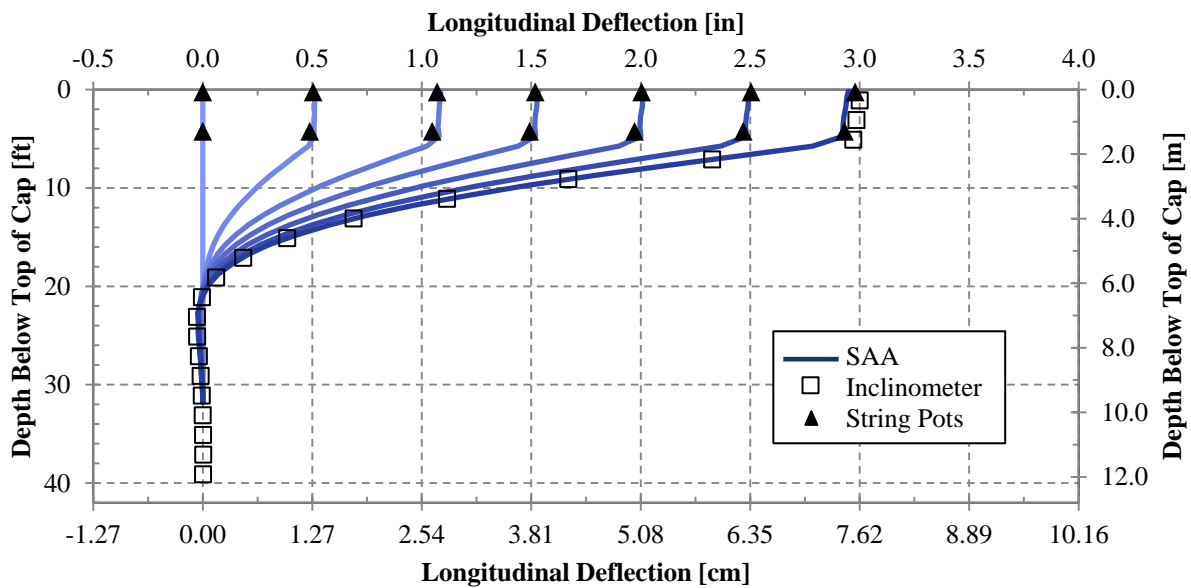


**FIGURE 24 Longitudinal deflection vs. depth curves from SAA data at various deflection increments for 45° skew unconfined test**

As noted previously, the inclinometer and shape arrays measured transverse deflections for the

north and south sides of the pile cap with depth. The measured transverse deflections at the top of pile cap

on both the north and south sides of the cap after the last deflection increment for each test are plotted in

Figure 25 from a plan view perspective, the transverse scale greatly exaggerated. By connecting these

points on the north and south sides, the rotation of the cap can be visualized. Although longitudinal

deflections of both actuators were kept relatively constant throughout the test, rotation and transverse

deflection were still affected by the skew angle. For the unconfined test, which developed greater

longitudinal resistance due to a greater amount of backfill, greater transverse movement developed than for the more confined MSE wall test. As seen in Figure 25, the unconfined test moved laterally about 0.46 inch on average, while the MSE test showed an average lateral pile cap movement of about 0.27 inch. In both cases these were greater lateral movements than the previous respective tests at lower skew angles. Both tests had similar pile cap rotation, with the unconfined test rotating the cap 0.03° counterclockwise and the MSE wall test rotating the cap 0.04° in the same direction.
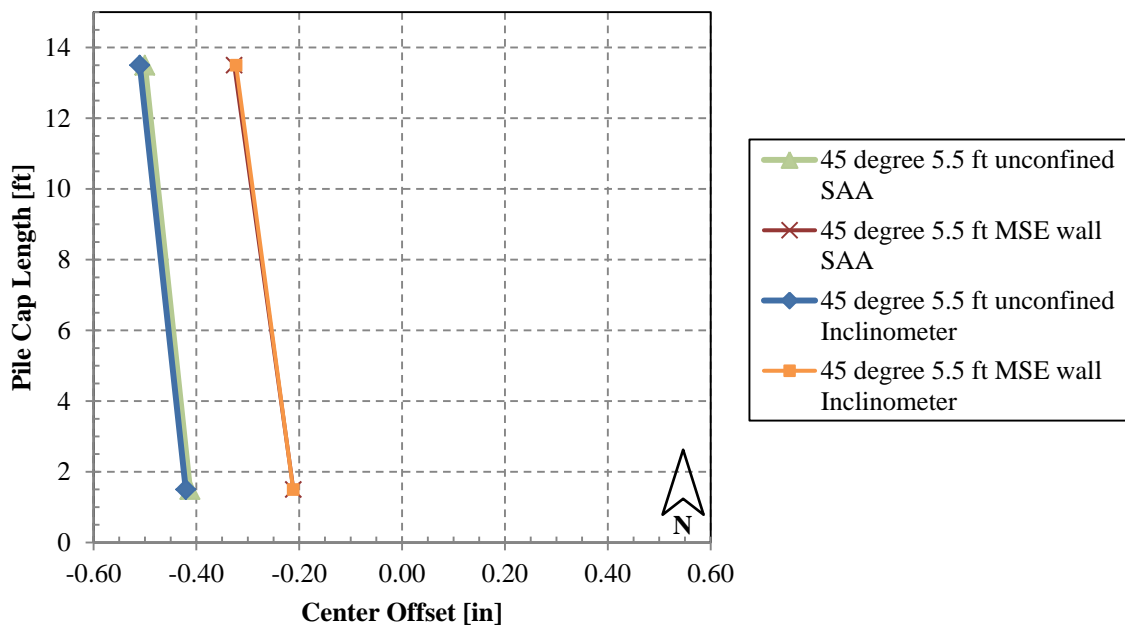


**FIGURE 25 Transverse pile cap deflection and rotation determined between north and south shape array and inclinometer data.**

**Pressure Distribution**

Figure 26 and 27 show the measured pressure distribution across the width of the pile cap for a series of pile cap displacement increments on both tests. Results are plotted from a plan view standpoint relative to the pile. Generally, the results show that the passive pressure is highest near the edges of the pile cap. This observation is consistent with expectations based on elastic theory.

(e)
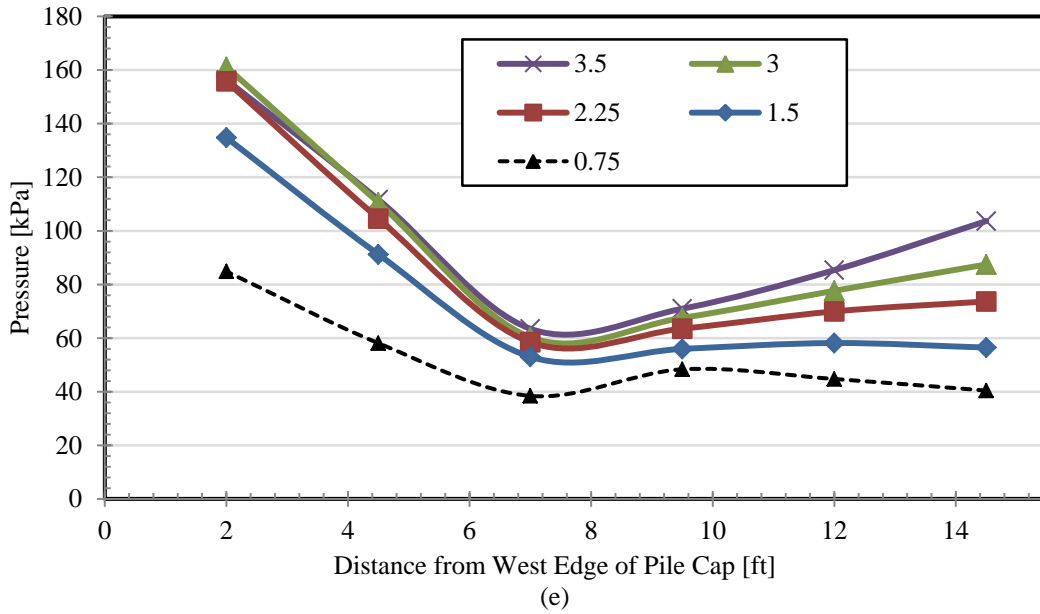
**FIGURE 26 Progression of horizontal pressure distribution with pile cap movement (in inches) for 45° MSE Wall skew test.**



Distance from West Edge of Pile Cap [ft]

(e)
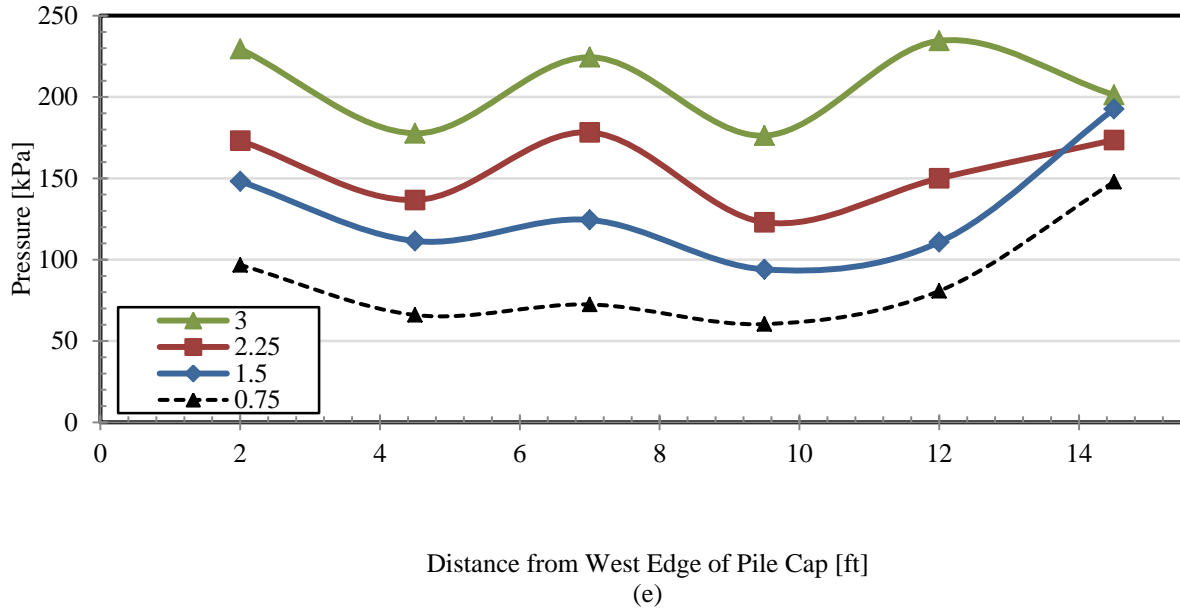
**FIGURE 27 Pressure distribution with pile cap movement (in inches) for 45° unconfined skew test.**

Although findings from displacement instrumentation reveal that the pile cap rotated slightly

counterclockwise and displaced to the left, rotation of the pile cap was greatly restricted by the actuators

and underlying piles. By significantly reducing this parameter, it can be implied that rotation is not the only cause of a variance in pressure distribution. Results from this study reveal that higher pressures can still develop on the obtuse side of the cap even if the pile cap is restrained and rotation is relatively small.

Figures 28 and 29 show comparisons of the passive force derived using the pressure plates and the passive force shown by the actuators. The pressure plate readings as shown assume no cohesion and a thus a triangular pressure distribution along the wall. In order to obtain a passive force from the pressure plate data, the initial readings were corrected for temperature, multiplied by 0.75 in order to find the average pressure along the height of the wall, then multiplied by their respective tributary areas and summed. As can be seen, the pressure plates agree well with the actuator readings during about the first inch of displacement for the unconfined test, and during the last two inches of displacement for the MSE wall test. These discrepancies appear to be due to either localized soil effects along the wall face or simply local deflection issues associated with the pressure plates. Pressure plates are notoriously for being somewhat erratic but the level of agreement between actuator and pressure plate readings is promising in that it suggests that patterns seen in the pressure plates are from reasonable data.
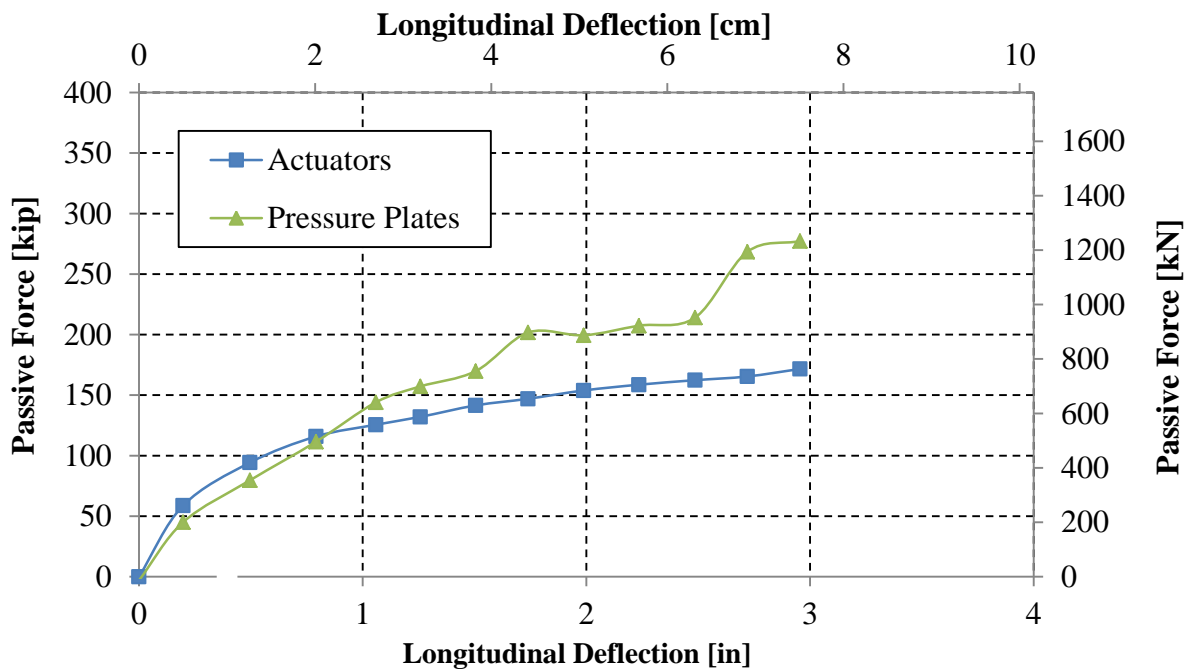


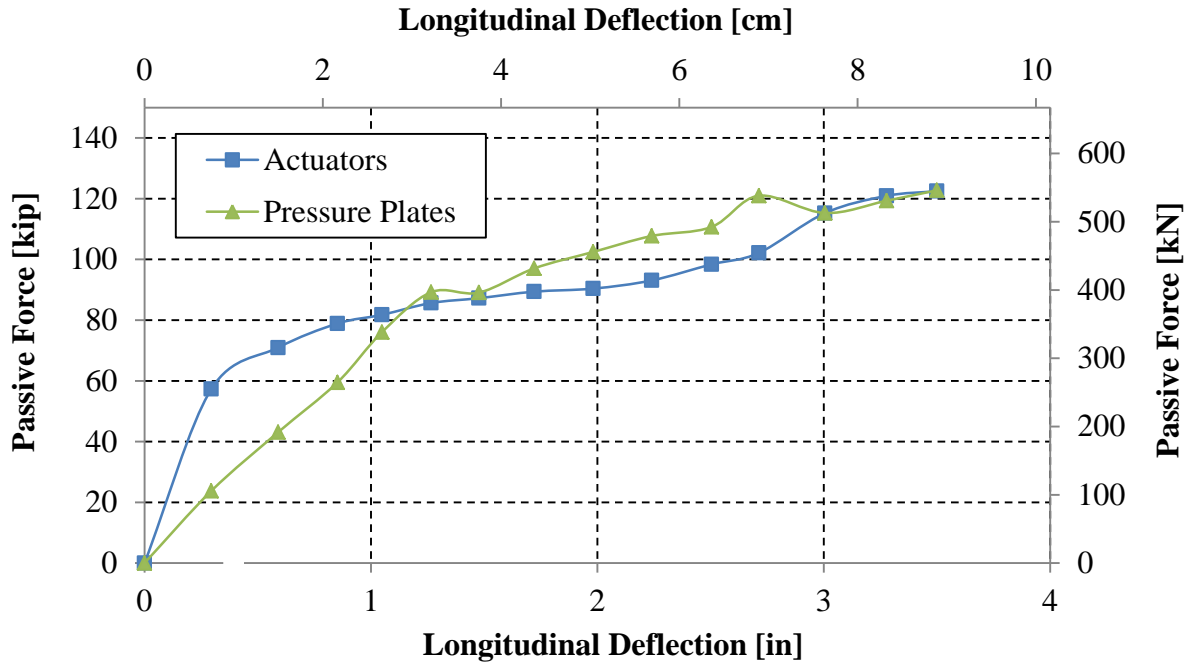**FIGURE 28 Passive force versus longitudinal deflection curves for 45° unconfined.**

**FIGURE 29 Passive force versus longitudinal deflection curves for 45° with MSE walls.**

## MSE Wall Deflection

Figures 30 and 31 illustrate the transverse deflection measured at the top of the MSE wingwalls. Figure 30 displays wall deflection plots imposed over the vertical heave pattern at test completion, while Figure 31 shows wall deflection plots with the horizontal backfill displacement vectors. Measurements suggest the general direction of horizontal backfill displacement was normal to the 45° skew abutment face (northeast direction) for the MSE wall test. The general direction of soil displacement explains the large deflections of the east MSE wall (≈ 2 in). Only small backfill displacements were detected toward the west MSE wall, which explains wall deflections of approximately 0.25 in at test completion.
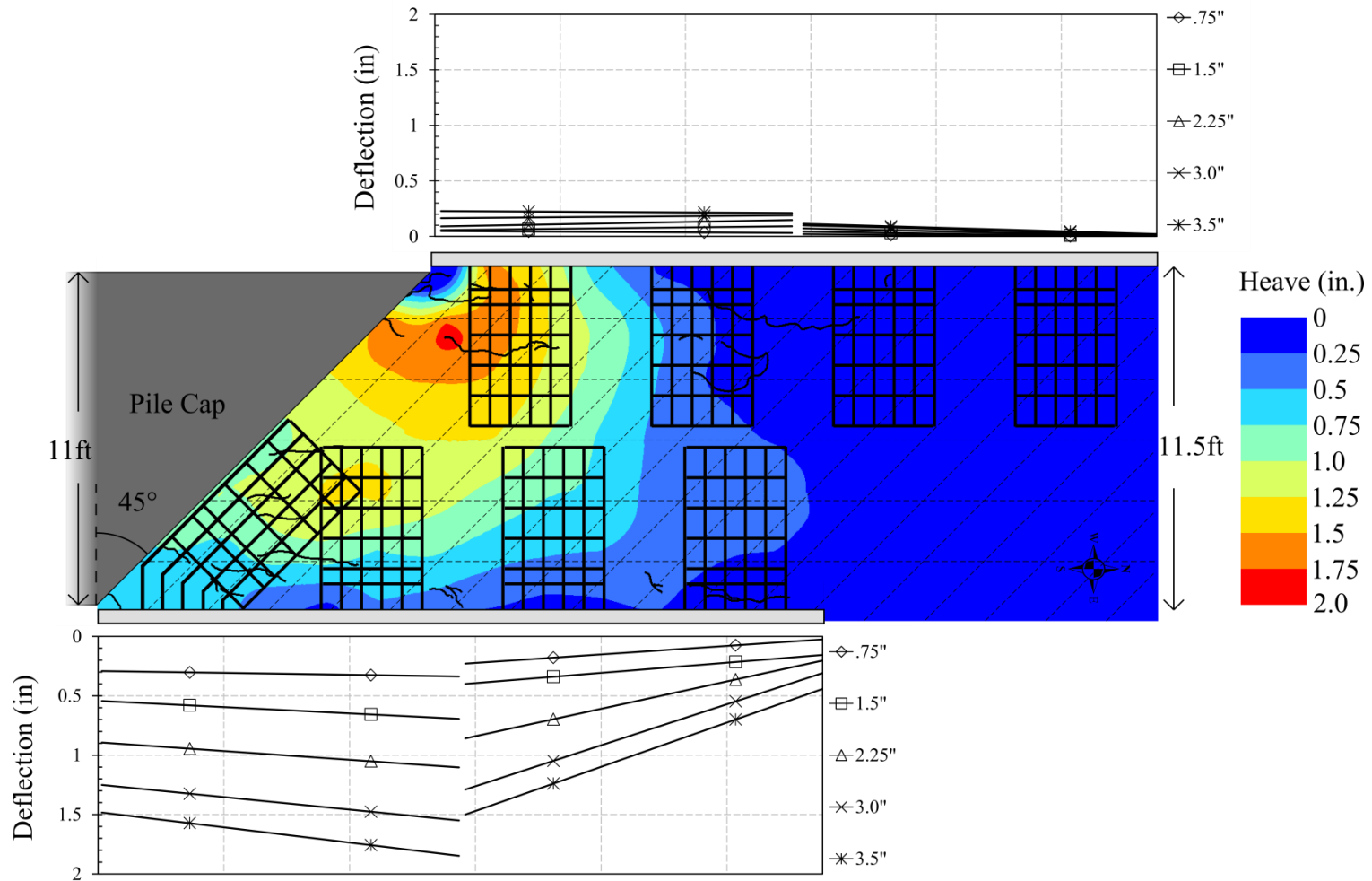
**FIGURE 30, MSE wall deflection with vertical heave and MSE grid overlay.**
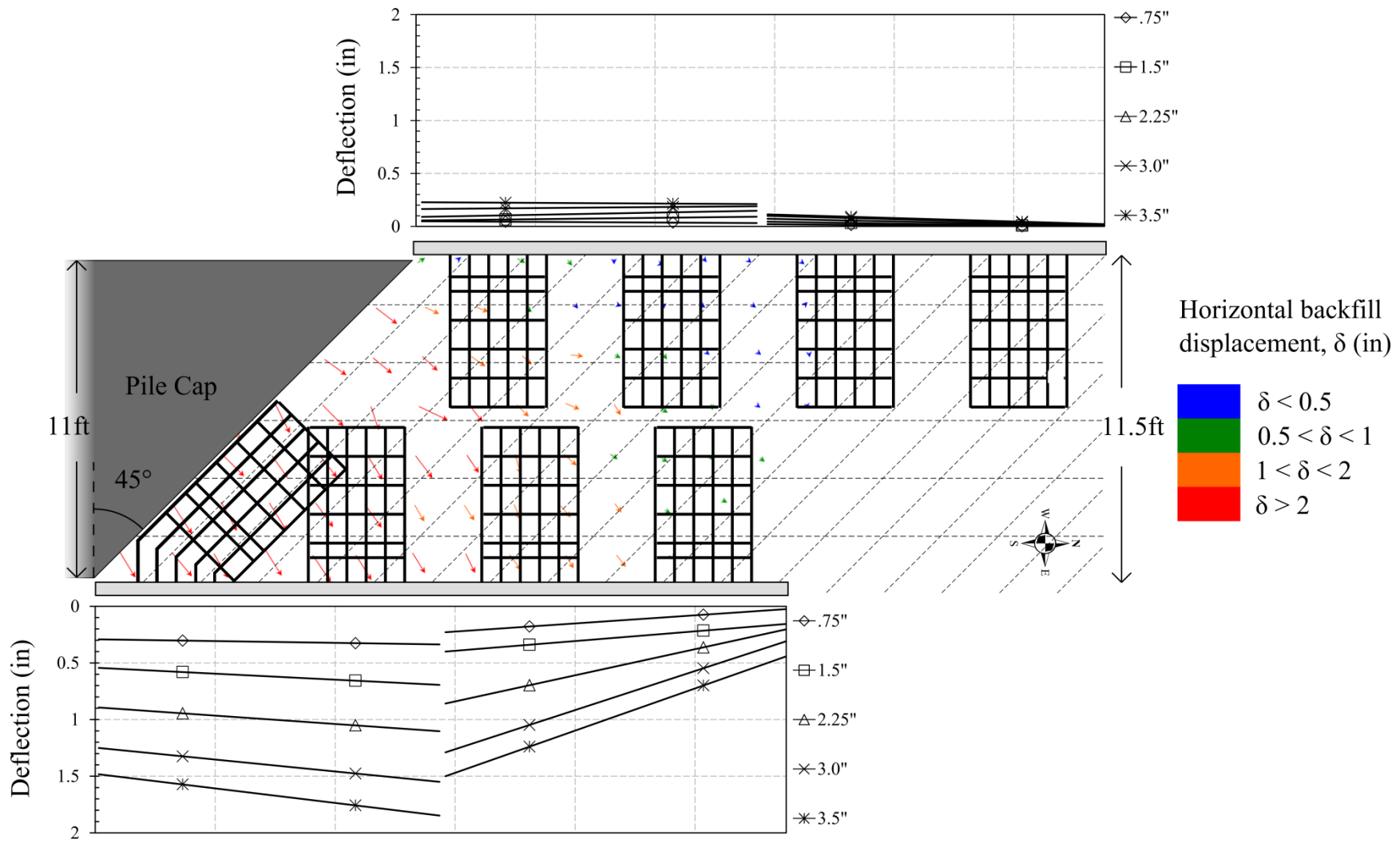
**FIGURE 31, MSE wall deflection with horizontal backfill displacement and MSE grid overlay.**
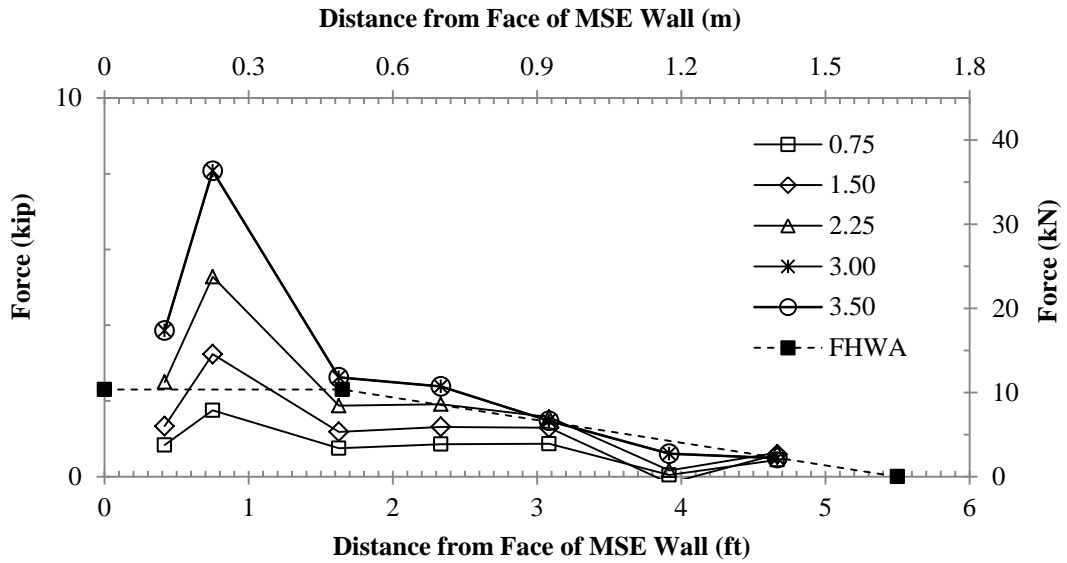
**MSE Grid Forces**

The following six figures (Figures 32 to 37) show the tensile force developed in the MSE reinforcements at five longitudinal cap displacements increasing up to the end of testing. Locations of each MSE grid are described on each plot. Tensile force was obtained by averaging the strain gauge readings on the top and bottom of the reinforcing grids along the length of the grid.

For the reinforcements on the west side of the abutment (see Figures 32 and 33), the tensile force progressively increases as the longitudinal displacement of the pile cap increases. The force in the reinforcements generally increases as distance to the wall face decreases and force mobilizes first at the end of the reinforcing grid. This force pattern indicates that load is being transferred to the reinforcement by friction as it is pulled outward relative to the surrounding soil. This is consistent with the displacement pattern shown in Figure 32 which shows the backfill soil moving eastward while the wall is moving westward. For the top west reinforcement (Figure 32), the measured tensile force pattern is very similar to the ultimate pull-out resistance predicted by the FHWA MSE wall design equations. This is consistent with the fact that the wall moved a little more than 0.25 inches at the top which is sufficient to mobilize friction. For the bottom reinforcement (Figure 33) the full tensile pull-out resistance predicted by FHWA has not been fully mobilized even for the largest longitudinal displacement of the pile cap. This is consistent with the fact that the wall rotated about its base so less displacement occurred near the bottom reinforcement grid. Nevertheless, the tensile force pattern appears to be developing in a manner consistent with the predicted pattern.

For the reinforcements on the east wall, (Figures 34 to 37) the force-distance curves are substantially different than for the west wall. This is a result of the fact that the soil around the reinforcements appears to be largely moving eastward as a block (see Figure 31) which completely contains the reinforcing grids in many cases. For example, the two reinforcement grids furthest north from the pile cap develop some tensile force at the far ends, but then the tensile force remains essentially flat or decreases. This pattern suggests that the soil is moving with the reinforcing grid or even moving

east relative to the grid throughout most of its length with the exception of the very end of the grid. Therefore, the reinforcement provides little resistance to the outward movement of the wall and it moves



**FIGURE 32 Force in West Top MSE Grids.**
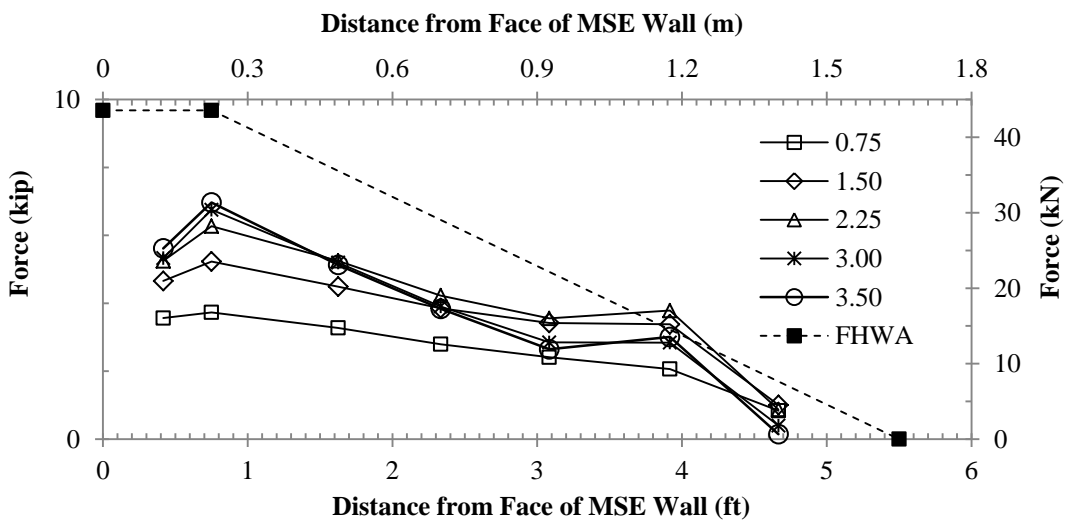


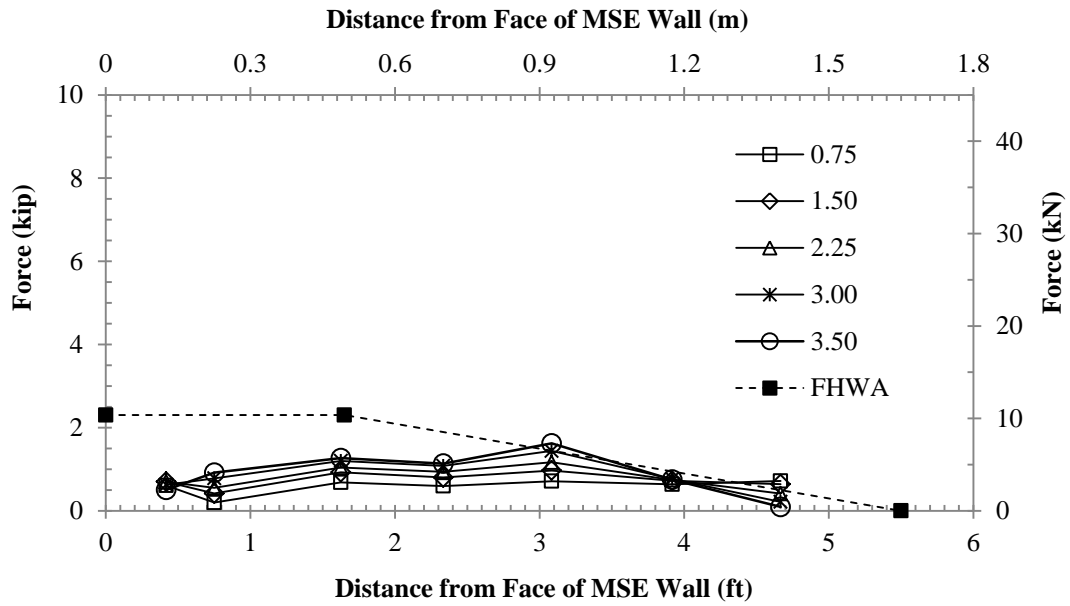**FIGURE 33 Force in West Bottom MSE Grids.**

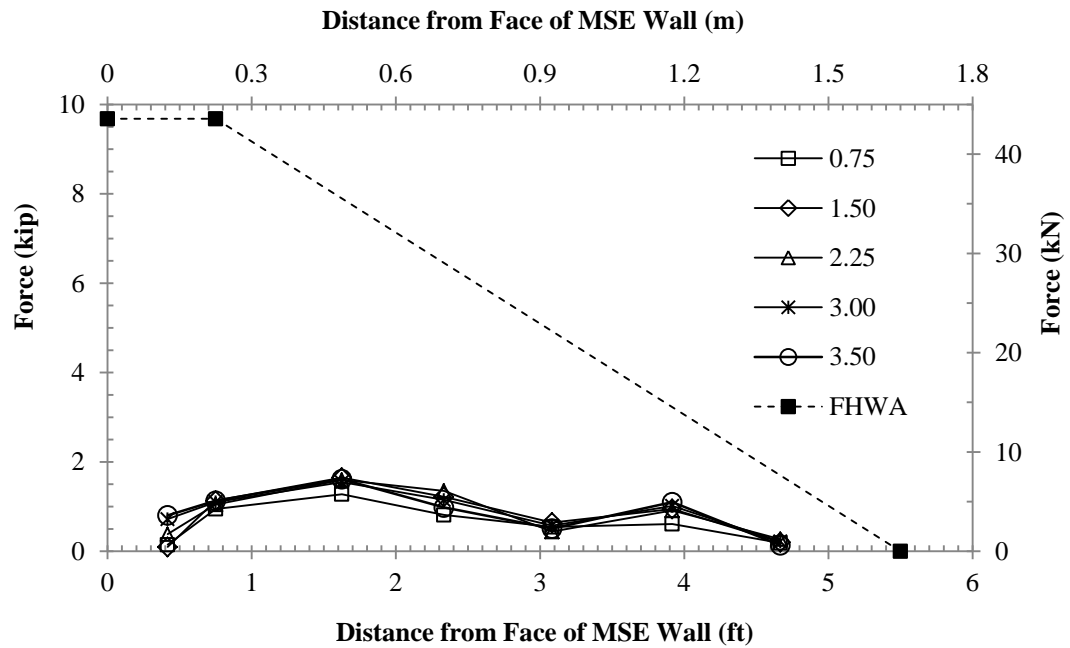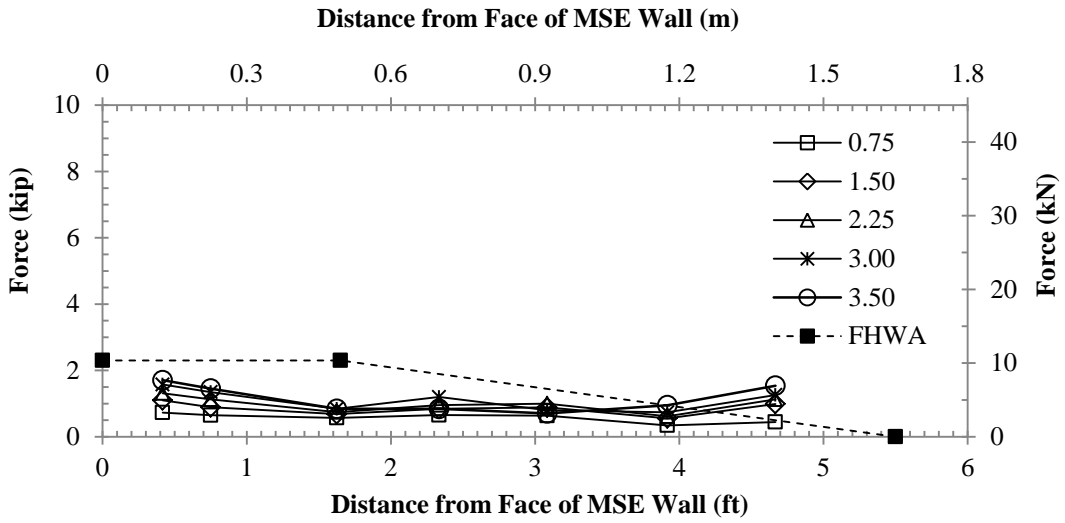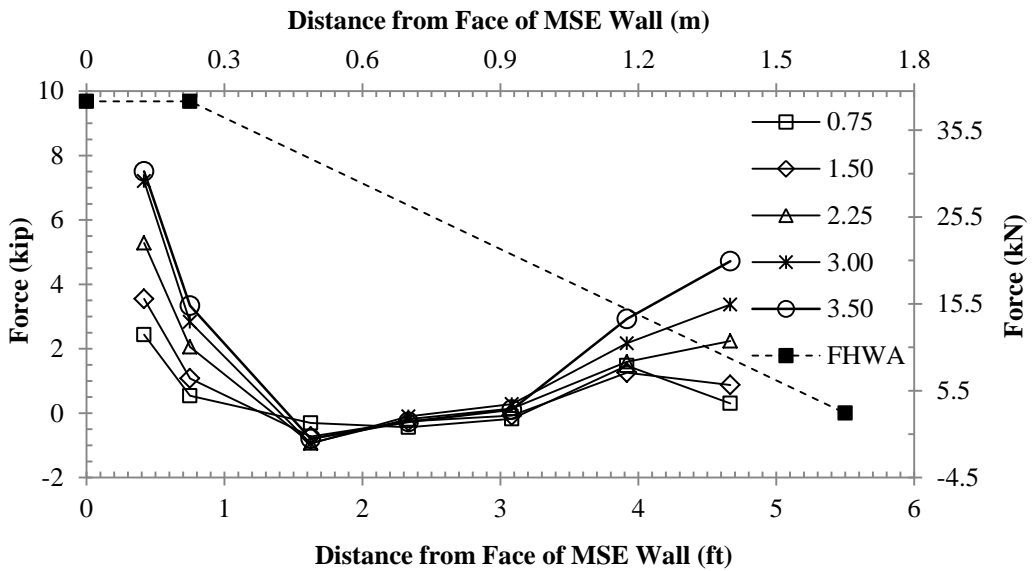**FIGURE 34 Force in East Top MSE Grids, farther from wall.**



**FIGURE 35 Force in East Bottom MSE Grids, farther from wall.**

**FIGURE 36 Force in East Top MSE Grids, nearer to wall.**



**FIGURE 37 Force in East Bottom MSE Grids, nearer to wall.**

progressively outward as the pile cap displaces longitudinally into the backfill as shown in Figure 31.

For the reinforcing grids on the east wall closest to the pile cap, the force in the middle section of the

reinforcement is still low, as was observed for the reinforcing grids further away from the pile cap.

However, the tensile force tends to increase at the ends of the grids. This effect is particularly true for the

bottom reinforcement (see Figure 37). As shown in Figure 31, the reinforcing grids are relatively close to

the face of the pile cap owing to the $45^0$ skew of the pile cap. It appears likely that the pile cap impinged

on the grid and that the measured tensile force at the ends of the reinforcing grids are a result of bending

rather than conventional axial force from soil-reinforcement interaction.

**Applied Shear Force vs. Transverse Displacement**

The relationship between the applied shear force ($P_T$) and transverse displacement is plotted in

Figure 38. The applied shear force was computed using Equation (3) and displacement values were based

on shape array measurements taken during testing. The shape arrays measured positive-east and negative-

west. The acute side of the skew was on the west.

Due to the greater total amount of backfill behind the unconfined test compared to the MSE wall

test, the shear force was greater than that on the MSE wall test (Figure 38 [A]). The higher shear force

also resulted in greater transverse movements toward the acute side of the pile cap. In Figure 38 [B] the

shear force for each cap has been normalized by the maximum shear force. In previous testing, the

maximum shear force occurred at the maximum longitudinal force. Since the shear force at the end of

loading for both tests shown is still increasing somewhat, the maximum longitudinal resistance was not

reached for these tests.
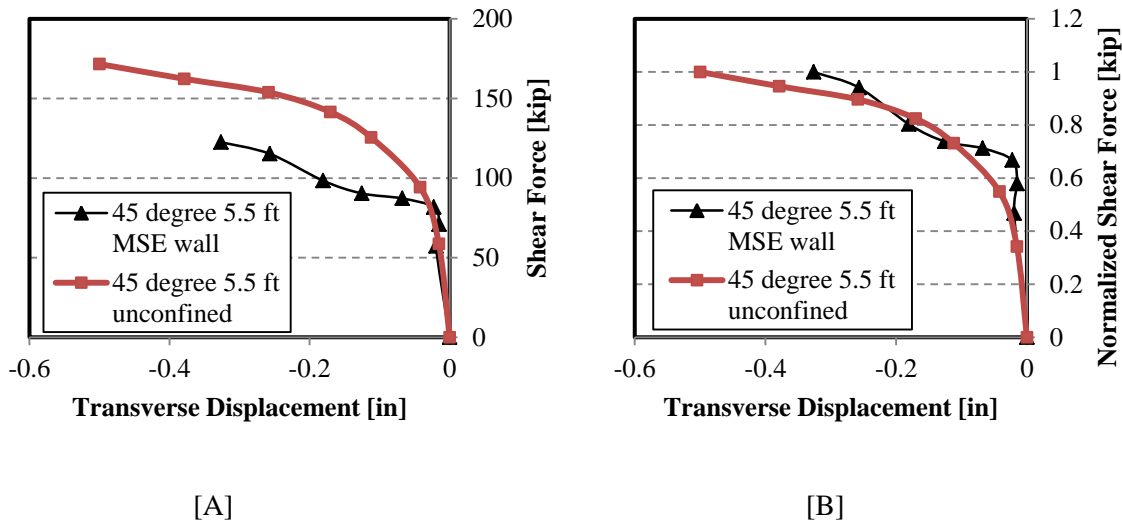
**FIGURE 38 [A] Applied shear force versus transverse displacement; [B] Normalized applied shear force versus transverse displacement.**

According to Duncan and Mokwa (2001), the amount of movement required to mobilize skin friction on an interface is typically between 0.10 and 0.25 inch. At a displacement of about 0.25 inch the shear force appears to be about 80% of the ultimate value. Therefore, the applied shear force could be greater than the shear resistance ($P_R$) provided by the abutment wall. In a subsequent report the shear resistance will be calculated once the interface friction angle and cohesion on the pile cap have been more accurately assessed.

**Shear Plane Geometry**

As can be seen from Figure 39, the 45° unconfined test failed showing a shear surface extending slightly below the base of the wall as in previous tests. However, in contrast to previous tests, the columns beyond four feet from the face showed no clear offsets indicating a failure surface. If we assume that a heave of 0.5 inch corresponds to the failure surface as in previous tests, we can assume that the failure mass would extend to a distance of about 18 feet from the face of the wedge at the surface.

No sand columns were placed during the 45° MSE Wall test due to the difficulty of digging the viewing trench without disturbing the MSE grids. A plot of the backfill vertical heave at test completion is provided in Figure 40.
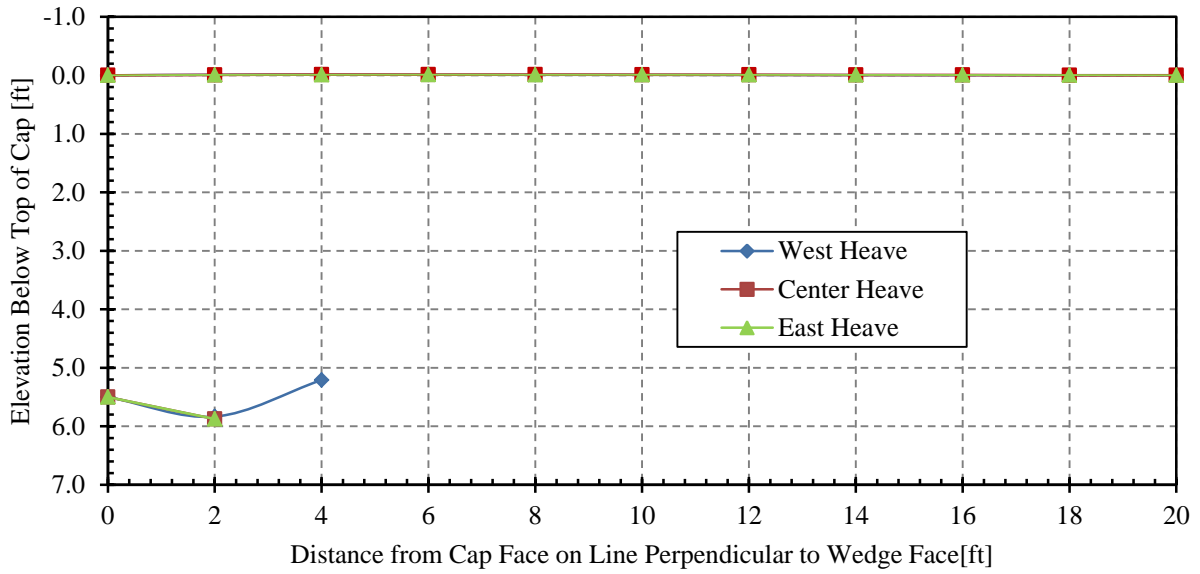
**FIGURE 39 Shear plane and heave geometry for 45° unconfined skew test.**
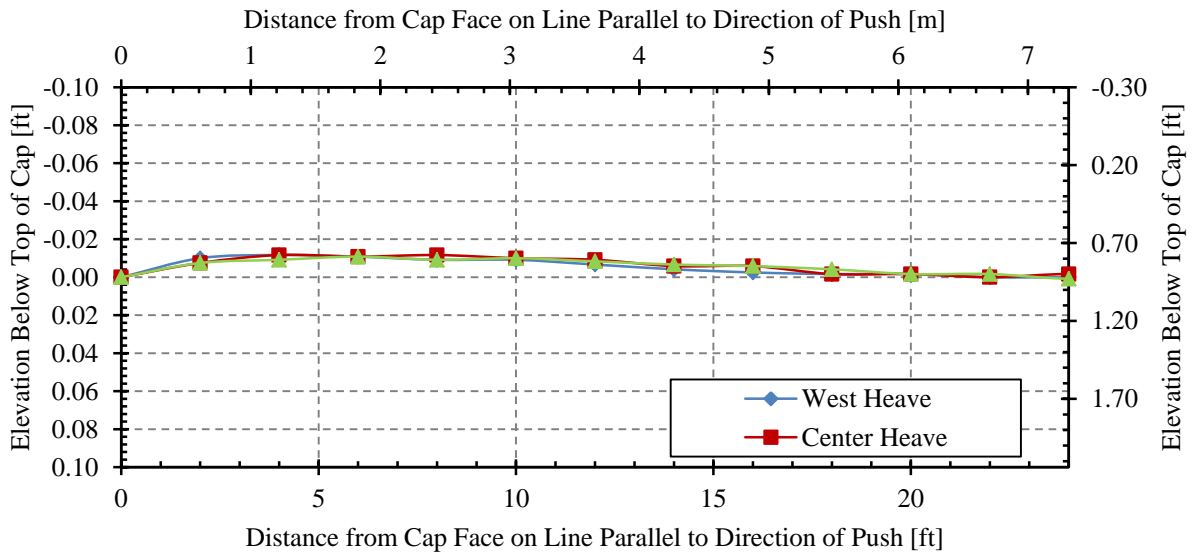


**FIGURE 40 Close up of ground surface heave for 45° unconfined skew test.**

## CONCLUSIONS

1. Tests with the 45⁰ skew abutment indicate that for both the unconfined backfill and the backfill with an MSE wingwall there was a significant reduction in passive force in relation to the 0⁰ skew abutment wall as observed in previous testing.

2. The reduction in passive force was generally consistent with that predicted by Rollins and Jessee (2013), although somewhat greater reduction was observed for the MSE backfill relative to the unconfined backfill.

3. For the unconfined backfill the displacement pattern was generally longitudinal, while for the MSE backfill the soil displaced almost uniformly normal to the skewed backwall. The displacement pattern for the MSE wall caused the East MSE wall to displace outward nearly 2 inches while the West wall only moved outward about 0.25 inches.

4. Since the backfill for the MSE wall moved largely as a block which extended beyond the length of the reinforcement, tensile force in the East reinforcements was relatively small. In contrast, tensile forces on the West wall were generally consistent with expectations based on the FHWA MSE wall design procedure.

5. Backfill heave was typically highest in front of the acute corner of the skewed abutment for both backfill geometries. Maximum backfill heave was approximately 3% of the fill height. The presence of the overlapping MSE reinforcements in combination with the outward movement on the east side of the wall led to somewhat lower heave in front of the obtuse side of the abutment wall than for the unconfined case.

6. Pressure plates on the face of the abutment backwall for both backfill geometries indicated that the pressures were greatest adjacent to the edges of the foundations and lowest near the center of the backwall as predicted by elastic theory. However, passive forces computed from the pressure cells did not always match up with the force measured by the hydraulic actuators. This suggests that the pressure cells may occasionally under- or over-register during the loading process.

## REFERENCES

AASHTO (2011). "Guide Specifications for LRFD Seismic Bridge Design." 5th Edition, 3-106.

Apirakyorapinit, P., Mohammadi, J., and Shen, J. (2012). "Analytical Investigation of Potential Seismic Damage to a Skewed Bridge." *Practice Periodical on Structural Design and Construction*, 16(1), 5-12.

Burke Jr., M. P. (1994). "Semi-Integral Bridges: Movements and Forces." 1-7.

Caltrans (2001). "Seismic Design Criteria Version 1.2." California Department of Transportation, Sacramento, California.

Duncan, J. M., and Mokwa, R. L. (2001). "Passive Earth Pressures: Theories and Tests." *Journal of Geotechnical and Geoenvironmental Engineering, ASCE*, 127(3), 248-257.

Elnashai, A. S., Gencturk, B., Kwon, O., Al-Qadi, I. L., Hashash, Y., Roesler, J. R., Kim, S. J., Jeong, S., Dukes, J., and Valdivia, A. (2010). "The Maule (Chile) Earthquake of February 27, 2010: Consequence Assessment and Case Studies." Department of Civil and Environmental Engineering, University of Illinois at Urbana-Champaign, 190.

Lee, K. L., and Singh, A. (1971). "Relative Density and Relative Compaction." *Journal of Soil Mechanics and Foundations Design*, 97(7), 1049-1052.

Mokwa, R. L., and Duncan, J. M. (2001). "Experimental Evaluation of Lateral-Load Resistance of Pile Caps." *Journal of Geotechnical and Geoenvironmental Engineering, ASCE*, 127(2), 185-192.

Rollins, K. M., and Cole, R. T. (2006). "Cyclic Lateral Load Behavior of a Pile Cap and Backfill." *Journal of Geotechnical and Geoenvironmental Engineering, ASCE*, 132(9), 1143-1153.

Rollins, K. M., Gerber, T., Cummins, C., and Herbst, M. (2009). "Monitoring Displacement vs. Depth in Lateral Pile Load Tests with Shape Accelerometer Arrays." *Proceedings of 17th International on Soil Mechanics & Geotechnical Engineering*, 3, 2016-2019.

Rollins, K. M., Gerber, T. M., Cummins, C. R., and Pruett, J. M. (2010). "Dynamic Pressure on Abutments and Pile Caps." *Report No. UT-10.18*, B. Y. University, U. D. o. Transportation, and F. H. Administration, eds., Utah Department of Transportation, 255.

Rollins, K. M., Gerber, T. M., and Heiner, L. (2010). "Passive Force-Deflection Behavior for Abutments with MSE Confined Approach Fills." *Report No. UT-10.15*, Utah Department of Transportation.

Rollins, K. M., and Jessee, S. (2012). "Passive Force-Deflection Curves for Skewed Abutments." *Journal of Bridge Engineering*, ASCE, 17(5).

Rollins, K. M., and Sparks, A. E. (2002). "Lateral Load Capacity of a Full-Scale Fixed-Head Pile Group." *Journal of Geotechnical and Geoenvironmental Engineering, ASCE*, 128(9), 711-723.

Shamsabadi, A., Kapuskar, M., and Zand, A. (2006 Published). "Three-Dimensional Nonlinear Finite-Element Soil-Abutment Structure Interaction Model for Skewed Bridges." *Paper presented at 5th National Seismic Conference On Bridges and Highways*, 1-10.

Shamsabadi, A., Rollins, K. M., and Kapaskur, M. (2007). "Nonlinear Soil-Abutment-Bridge Structure Interaction for Seismic Performance-Based Design." *Journal of Geotechnical and Geoenvironmental Engineering, ASCE*, 133(6), 707-720.

Steinberg, E., and Sargand, S. (2010). "Forces in Wingwalls from Thermal Expansion of Skewed Semi-Integral Bridges." *Report No. FHWA/OH-2010/16*, Prepared by Ohio University for Ohio Department of Transportation, Athens, OH, 87.

Strassburg, A. N. (2010). "Influence of Relative Compaction on Passive Resistance of Abutments with Mechanical Stabilized Earth (MSE) Wingwalls." M.S. Thesis, Brigham Young University, Provo, UT.

Unjohn, S. "Repair and Retrofit of Bridges Damaged by the 2010 Chile, Maule Earthquake." *Proc., International Symposium on Engineering Lessons Learned from the 2011 Great East Japan Earthquake*, Tokyo, Japan.